CHALMERS

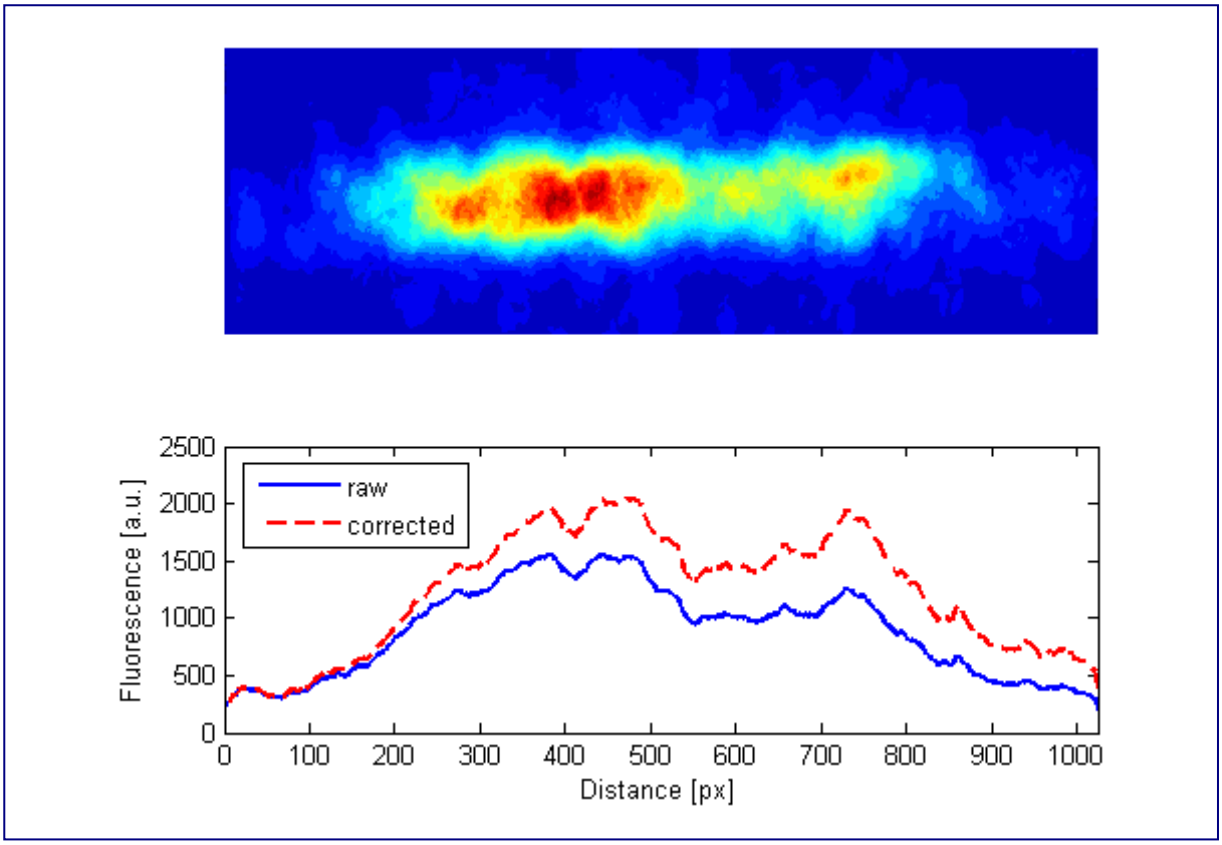

Nitric oxide measurements in DME flames using laser induced fluorescence

Master's Thesis in the Erasmus programme

CESAR ALVAREZ

Department of Applied Mechanics
Division of Combustion
CHALMERS UNIVERSITY OF TECHNOLOGY
Göteborg, Sweden 2011
Master's Thesis 2011:08

MASTER'S THESIS 2011:08

Nitric oxide measurements in DME flames

Master's Thesis in the Erasmus programme

CESAR ALVAREZ

Department of Applied Mechanics
Division of Combustion
CHALMERS UNIVERSITY OF TECHNOLOGY
Göteborg, Sweden 2011

Nitric oxide measurements in DME flames using laser induced fluorescence

Master's Thesis in the Erasmus programme
CESAR ALVAREZ

Master's Thesis 2011:08
ISSN 1652-8557
Department of Applied Mechanics
Division of Combustion
Chalmers University of Technology
SE-412 96 Göteborg
Sweden
Telephone: + 46 (0)31-772 1000

Cover:
Nitric oxide fluorescence at 8 ms after start of injection and vertical integration.

Department of Applied Mechanics
Göteborg, Sweden 2011

Nitric oxide measurements in DME flames using laser induced fluorescence

Master's Thesis in the Erasmus programme

CESAR ALVAREZ
Department of Applied Mechanics
Division of Combustion
Chalmers University of Technology

ABSTRACT

The aim of the work described in this report is to show and understand the nitric oxide (NO) formation in a dimethyl ether combusting spray. In order to achieve it, optical measurements using laser induced fluorescence (LIF) have been performed in a combustion chamber.

The measurements have been carried out using A←X (0, 1) excitation around 226 nm using a dye laser pumped by a Nd:YAG. The fluorescence has been mainly detected in A→X (0, 2) bands using an intensified charge-coupled device camera. Measurements at different times after the start of injection and at different distances from the nozzle have been executed. Later, injection pressure has been increased to quantify its effect on NO formation, measuring at different times at 90 mm from the nozzle. Images from the fluorescence have been processed, using experimental models and corrections for attenuation of the laser beam.

The results show that the NO maximum fluorescence (and thus concentration) takes place around 7-8 ms after start of injection at distances far from the nozzle, where the spray is fully developed. The results also show that the NO formation is uniform along the flame, although more fluorescence can be noticed on the lean sides of the flame. Increasing the injection pressure resulted in less remaining NO at that distance from the nozzle.

The presence of atomic oxygen in the DME molecule is thought to be the cause of the NO uniform formation. On the other hand, although the results showed a reduction of NO when increasing injection pressure, it is thought that the overall formation must be higher.

Key words: Nitric oxide (NO), dimethyl ether (DME), emission, absorption, laser induced fluorescence (LIF).

Contents

Preface

The current project represents a part of a research project about DME in the diesel process performed by Combustion division at Chalmers University of Technology. Preparations for the experiments were carried out from December 2010 until May 2011. Measurements started on May 2011 and finished on June 2011.

The experiments were financed by Combustion Division at Chalmers University of Technology. They were carried out in Cell G lab, property of the Division, in collaboration with professor Mats Andersson as examiner and PhD student Henrik Salsing as supervisor. Other workers in the Division such as Alf Magnusson, Eugenio de Benito and Raul Ochoterena deserve to be mentioned as well. I would like to thank all of them for their help.

Göteborg, June 2011

Cesar Alvarez

Notations

Roman upper case letters

A	Area of the laser beam/sheet. Attenuation
$A_{2\to1}$	Spontaneous emission rate
B	Rotational constant of the molecule
$B_{1\to2}$	Einstein coefficient for stimulated absorption
C_{exp}	Experimental constant
E	Energy
F	Fluorescence
I_{ν}	Laser excitation irradiance
I	Light intensity
J	Rotational quantum number
N_i	Population at the i energy level
N	Number of molecules
P	Predissociation rate
$Q_{2\to1}$	Collisional quenching rate
T	Temperature
Tr	Transmittance
$W_{2\to i}$	Photoionization rate
$[X]$	X concentration

Roman lower case letters

$b_{1\to2}$	Stimulated absorption coefficient
$b_{2\to1}$	Stimulated emission coefficient
c	Speed of light
f	Boltzmann fraction
g	Degeneracy. Overlap integral
h	Planck constant
k	Boltzmann constant
l	Length of the beam/sheet from which fluorescence is observed
t	Time
v	Vibrational quantum number

Greek upper case letters

Ω	Collection optics solid angle
Φ	Stern Volmer factor

Greek lower case letters

σ	Collisional cross section
ν	Frequency
ρ	Density
χ	Molar fraction

Other symbols

$\rightarrow$	Direction of the electronic transition (emission)
$\leftarrow$	Direction of the electronic transition (excitation)

1 Motivation and objectives

Nowadays, engine manufacturers have to fulfil legislation requirements about local emissions like nitric oxide and soot; thereby most of the research in combustion is focused on reducing these. On the other hand, new fuels like dimethyl ether are becoming more important in this field since they allow reduction in emissions. DME provides a good reduction in particle matter, while keeping a relatively good performance in Diesel engines comparison with fossil fuels. The NO production in DME combustion needs to be reduced as well to make it a suitable substitute for diesel fuel.

In order to reduce NO emissions, understanding about how it is formed is required. Optical methods have been used for several years to achieve that, as they provide information without interfering in the combustion process. However, these methods require optical access to the combustion environment (engine, bomb...) and need physical understanding of the phenomena to get accurate results.

Therefore, the aim of the work is to know how nitric oxide is formed in a DME flame, using an optical method like laser induced fluorescence. The objective is to analyze where and when this formation occurs within the flame and how some parameters like injection pressure affect it.

2 Background

2.1 Introduction to LIF

Laser induced fluoresce (LIF) spectroscopy is an incoherent diagnostic technique which allows detection and measurement of species in chemical environments. It consists of illuminating a sample with light coming from a laser source and catching the fluorescence emitted by the sample with a recording device.

It has widely been used in investigation of combustion species formation since it is a non intrusive measurement method, linear and very sensitive. However it has some drawbacks: it is necessary optical access to the combustion process, and as a great amount of intermediate species is formed during the combustion process, interferences usually occur as it will be explained later in the report [1].

2.1.1 LIF physical basis

LIF is based on rotational and vibrational energy transitions between an electronic excited and a ground state of a molecule. The underlying principle is that molecules can only absorb and emit radiation (photons) at very specific and characteristic wavelengths (energies) according to quantum theory [3]. When the molecule is excited at a fixed wavelength, it can absorb photons by changing its rotational and vibrational energy levels. This energy absorption is followed by an emission of photons in a wide range of wavelengths, hence decaying its energy state [1, 2]. All processes take place in a short amount of time (picoseconds).

In order to use LIF for measurements the emission spectra of the molecule must be known, which is not always possible because predissociation is prone to happen in the excited level [1].

In conclusion, energy transitions and molecular spectra have to be studied previously.

2.1.2 Molecular energy levels

In order to understand the energy transfer between different states it is necessary to know how the energy levels are distributed in a molecule (in this case NO):

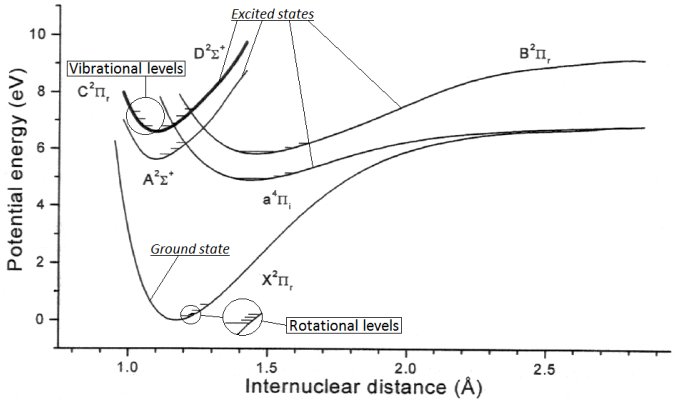

Figure 1. Distribution of energy states in a nitric oxide molecule. [Adapted from 4]

The molecular energy is composed by electronic, vibrational and rotational energy, where the amount of an energy transition in each level is approximately given by the next correlation [5]:

$$\Delta E_{electronic} \approx \Delta E_{vibrational} \cdot 10^3 \approx \Delta E_{rotational} \cdot 10^6 \quad (1)$$

Two electronics states, ground and excited, are represented in Figure 1. These states are usually represented by an expression like ${}^{2S+1}\Lambda^x$; where:

- *S:* Resultant spin of the molecule. Possible values are: 1/2, 3/2…
- *Λ:* Total electronic orbital angular momentum quantum number. Possible values are 0, 1, 2, 3… represented by Greek letters: Σ, Π, Δ, Φ… respectively.
- *x:* Values + or – depending whether the electronic wave functions are symmetric or antisymmetric.

Then an example of an electronic state could be ${}^2\Pi$. It is common to represent the ground state of a molecule preceded by the letter X and the excited states by an A (1st excited state), B (2nd excited state), C (3rd excited state), etc. if they have the same multiplicity as the ground state (spin-allowed transitions) or a, b, c, etc. if they have different multiplicity ("forbidden transitions"). Thus, in the previous example, assuming that it is the ground state of a given molecule, the ground electronic level can be written as follows: $X\,{}^2\Pi$.

On the other hand, vibrational and rotational levels are represented by their respective quantum numbers *v* and *J*, and a prime or double prime symbol depending on whether they are in the ground electronic state (*v''*, *J''*) or the excited one (*v'*, *J'*). These quantum numbers achieve integer values and, are not only useful to represent transitions, but also quantify the amount of energy according to Planck theory:

$$E_{rotational} = hcBJ(J+1) \quad (2)$$

$$E_{vibrational} = h\nu\left(\nu + \frac{1}{2}\right) \quad (3)$$

It needs to be remarked that these transitions are only decoupled in molecules with permanent dipole moment [1].

Depending on the increase in the rotational quantum number (*J*) between the ground and excited state, rotational transitions are usually represented by capital letter according to Table 1:

Table 1. Nomenclature of rotational transitions in molecules.

Transition	P	Q	R
ΔJ = J'–J''	-1	0	1

As it was introduced in the previous paragraph, after excitation and absorption, the molecule spontaneously emits a photon (fluorescence). Since the molecule energy can decay to more than one rotational/vibrational level, the fluorescence might be emitted in a different wavelength from the stimulating signal and therefore be easily detected after filtering [3]. Nevertheless, other competing phenomena happen when exciting a molecule, such as:

- Predissociation: the molecule fragments at energies lower than the dissociation limit if the energy states overlap. The dissociation limit is a constant energy above which a diatomic molecule spontaneously dissociates.

- Photoionization: the incoming light takes out one or more electrons.
- Collisional quenching: the fluorescence intensity decays because of the contact with other molecules in a combustion environment. This is the main competing state in NO fluorescence at high pressures. Figure 2 shows how quenching interacts with laser excitation and fluorescence:

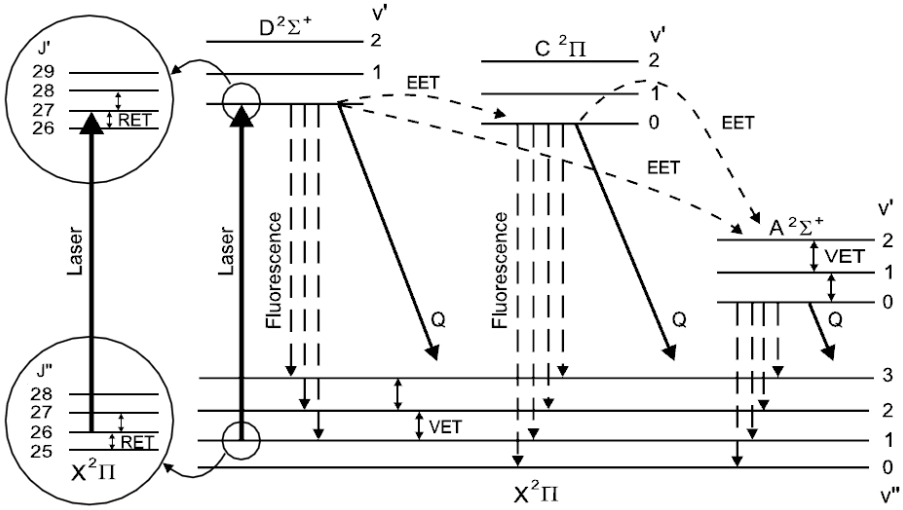

Figure 2. Energy transfer paths between several states of a molecule. [3]

2.1.3 Rotational and vibrational spectra

The energy levels named above correspond with different wavelengths according to Quantum Theory. Therefore another representation can be useful. This consists on representing the wavelength vs. the excitation/absorption/emission fluorescence intensity as it is shown in Figure 3:

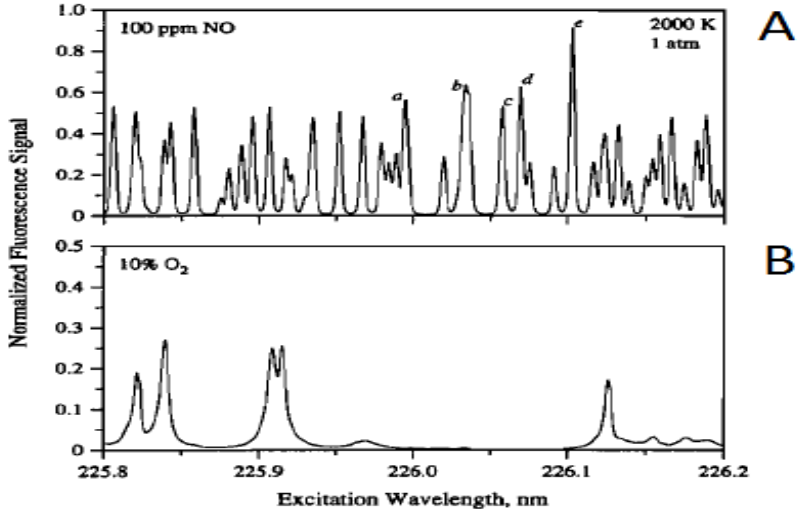

Figure 3. NO excitation spectra (A) and O_2 excitation spectra (B) [6]

At the given resolution, the vibrational transitions are represented by peaks in the spectrum. Inside the vibrational transitions the rotational transitions can be visualized by zooming in. When a mixture of several species is studied, as it happens in combustion analyses (and also in Figure 3), their spectra interfere. However, by knowing their spectra separately, it is possible to recognize each one.

In an ideal case the peaks would be infinitely sharp, but broadening phenomena take place. This broadening can be:

- Doppler broadening due to Doppler Effect, especially at low pressures, around atmospheric pressure.
- Pressure broadening. It happens as absorption and emission radiations are interrupted by collisions at high pressures, like the pressures in a combustion environment. The higher the pressure, the stronger the broadening.
- Predissociation broadening, caused when some molecules dissociate before rotational energy transfers occur.

Gaussian (Doppler) and Lorentzian (Pressure) lineshapes have already been used in modelling these effects in the spectra. When more than one phenomenon is considered (especially at medium pressures), a Voigt lineshape, convolution of a Lorentzian and a Gaussian profile, can be adjusted for the total broadening [1, 2, 3].

2.1.4 Population distribution

If the intensity of the fluorescence emitted is measured, it is possible to determine the number of molecules in the excited (N_{upper}) state since both variables are proportional. In most experiments, more than one rotational level interacts, yet in order to give a simplified overview let us summarize the two level model proposed by Eckbreth:

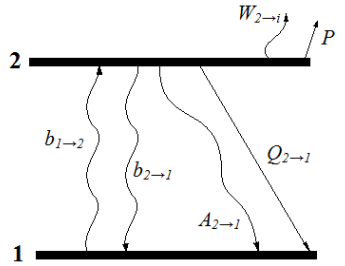

Figure 4. Two energy level model and transitions.

According to Figure 4, equations that govern the population distribution are derived:

$$\frac{dN_1}{dt} = -N_1 b_{1\to 2} + N_2\left(b_{2\to 1} + A_{2\to 1} + Q_{2\to 1}\right) (4)$$

$$\frac{dN_2}{dt} = N_1 b_{1\to 2} - N_2\left(b_{2\to 1} + A_{2\to 1} + Q_{2\to 1} + P + W_{2\to i}\right) (5)$$

Assuming that, before the excitation there is no population in the excited level in the beginning and that excitation irradiance is low enough to consider a linear regime, a relation between the fluorescence and the initial population is derived [1]:

$$F = \frac{h\nu}{c}\frac{\Omega}{4\pi} l A N_1^0 B_{1\to 2} I_\nu \Phi \ (6)$$

Although in this simplified model the initial ground population ($N_1{}^0$) matches the total population (N_T) as there is no other competing state, in more complex models this fact does not occur and both population are linked by the Boltzmann fraction:

$$\frac{N_1^0}{N_T} = \frac{g_1 e^{-E_1/kT}}{\sum_i g_i e^{-E_i/kT}} \ (7)$$

2.2 NO detection

There is not only one scheme for excitation-detection in NO analyses and several methods have been studied and developed so far. The majority of these methods are based in A←X and D←X excitation schemes. Therefore, explanations of these methods are given in the next paragraphs:

2.2.1 D←X excitation

Only D←X excitation between vibrational levels 0 and 1 has been used in research until now. NO D←X (0, 1) system, as it is shown in Figure 5, excites the sample at wavelengths between 192nm and 195nm which can be achieved with a tunable ArF laser. Most experiments have been carried out at a wavelength 193.38 in the $R_1(26)+Q_1(32)$ level, firstly reported by Andresen *et al.* [7]. Another excitation scheme was proposed by Brugman et al. at 193.588 in the $R_1(23.5)/Q_1$ (29.5) bands. The radiation was detected in the D→X (0, 3) at 208nm (Figure 6). The main drawback when using this method is the attenuation of the laser signal due to hot CO_2, scattering, soot particles and polyaromatic hydrocarbons (PAH). [8]

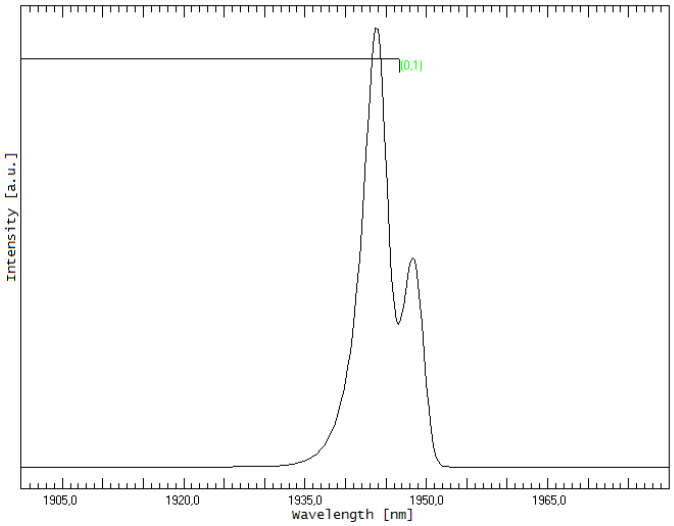

Figure 5. Nitric Oxide D←X excitation spectrum simulation using LIF–Base.

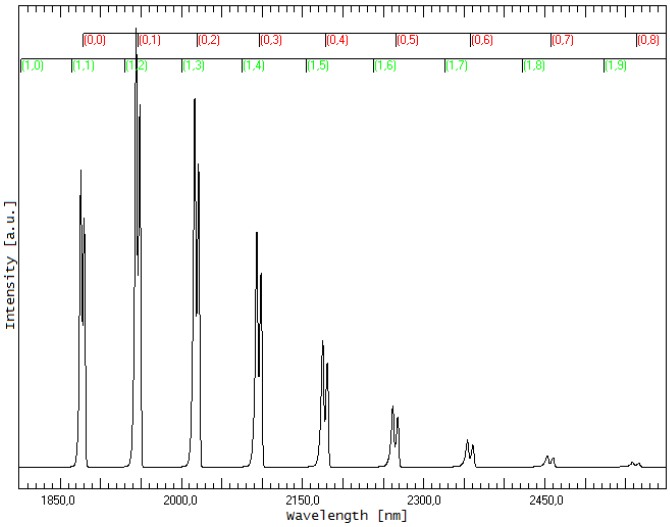

Figure 6. Nitric Oxide D→X emission spectrum simulation using LIF–Base.

2.2.2 A←X excitation

Regarding the A←X excitation, three different schemes have been used so far in NO detection. Those are NO A←X (0, 0), certainly the most widely used technique; NO A←X (0, 1) and NO A←X (0, 2).

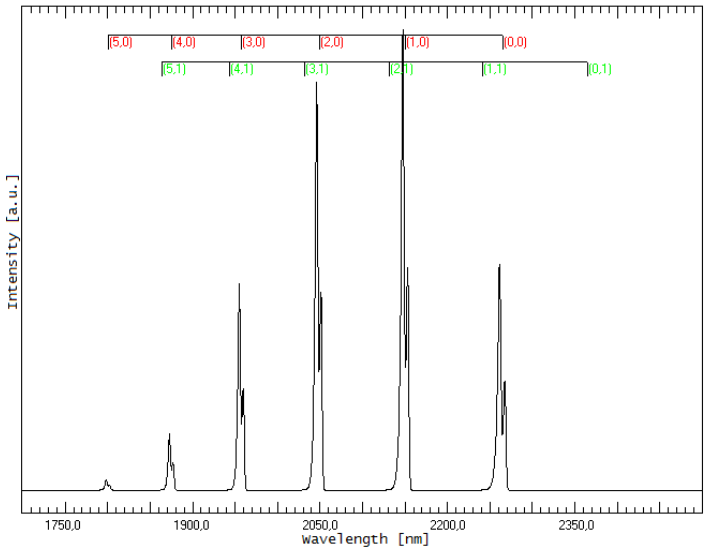

Figure 7. Nitric Oxide A←X excitation spectrum simulation using LIF–Base.

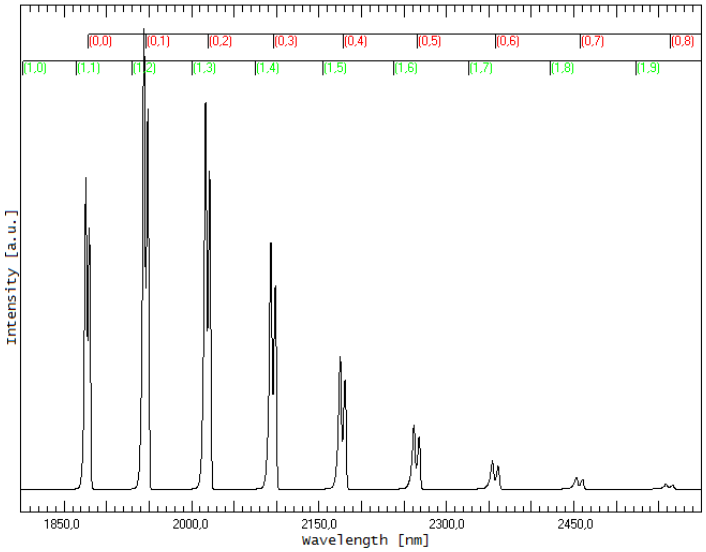

Figure 8. Nitric Oxide A→X emission spectrum simulation using LIF–Base.

2.2.2.1 A←X (0, 0)

This scheme uses excitation wavelengths of 224-227nm according to the excitation spectra in Figure 5. The resulting fluorescence gathers wavelengths between 220 and 300nm [6], therefore detection can be performed using a narrow bandpass around the (0, 1) and (0, 2) emission [9]. In these transitions, the signal is stronger and the O_2 interference can be minimized. Table 2 summarizes some illustrative experiments carried out using A←X (0, 0) excitation in methane premixed flames:

Table 2. A←X (0, 0) excitation schemes. [11]

Researcher	$\lambda_{excitation}$ (nm)	Rotational excited levels	Vibrational collection
Bessler (High T)	224.82	$R_1+Q_{21}(26.5)$ $Q_2+R_{12}(34.5)$	(0,1-2)
Bessler (Low T)	226.87	$P_2+Q_{12}(1.5\text{-}4.5)$	(0,1-2)
Sick	225.25	$R_1+Q_{21}(21.5)$	(0,1-2)
Laurendau	225.58	$Q_2(26.6)$	(0,1-2)
DiRosa	226.07	$P_1(23.5)$ $Q_1+P_{21}(14.5)$ $Q_2+R_{12}(20.5)$	(0,1-5)

There are many other excitation techniques, most of them using the same excitation levels or wavelengths but with different fuels.

It is worth to mention the model proposed by DiRosa [6] since it achieves an important reduction in oxygen interference: The so-called Schumman-Runge bands (B←X vibrational transitions) of the O_2 overlap the wavelength range of the NO emission. These interference needs to be quantified in order to achieve reliable measurements.

This strategy offers an acceptable signal strength and is suitable for high pressure combustion environments, with small flames [11]. Therefore this is the method used in the current work.

2.2.2.2 A←X (0, 1)

A←X (0, 1) excitation strategy uses wavelengths in the 233-237nm region. The detection is usually performed either in:

- A→X (0, 0) band using a bandpass filter between 217 and 232nm or
- A→X (0, 2) and A→X (0, 3) bands using a bandpass filter between 243 and 263nm.

Table 3 gathers some experiments carried out with this scheme:

Table 3. A←X (0, 1) excitation schemes. [11]

Researcher	$\lambda_{excitation}$ (nm)	Rotational excited levels	Vibrational collection
Bessler (A)	235.55	$R_1+Q_{21}(16.5)$ $P_2+Q_{12}(32.5)$ $P_{21}(22.5)$ $O_{12}(40.5)$	(0,2-3)
Bessler (B)	235.87	$P_1(25.5)$ $R_1+Q_{21}(11.5)$ $Q_1+P_{21}(17.5)$	(0,2-3)
Jamette *et al.*	236.22	$R_1+Q_{21}(22.5)$ $Q_1+P_{21}(8.5)$ $Q_2+R_1(17.5)$	(0,2-3)

Although this excitation-detection strategy has not been very popular, its increased wavelength compared A←X (0, 0) results in a lower attenuation, providing relatively strong signals (about one third of A←X (0, 0)). Nevertheless it can increase interferences from PAH [11].

2.2.2.3 A←X (0, 2)

Here the excitation is around 248nm, collecting emissions can be done in the:

- A→X (0, 0) and A→X (0, 1) bands using a bandpass between 220 and 240nm or
- A→X (0, 3) and A→X (0, 4) bands using a bandpass between 255 and 275nm.

Table 4. A←X (0, 2) excitation schemes. [11]

Researcher	$\lambda_{excitation}$ (nm)	Rotational excited levels	Vibrational collection
Schulz	247.95	O_{12}	(0,0-1)
Hildelbrand	247.94	O_{12}	(0,1)

The major drawback in this method is the weak signal strength. However, it reduces attenuation and interference from PAH [11].

2.3 NO formation

2.3.1 Basics about Diesel combustion

Combustion in a Diesel spray is a complicated process involving thermodynamics (heat release, heat transfer...), chemistry (around 10000 species and 1000 reactions) and fluid motion (turbulence, spray development...).

When the needle of the injector lifts up the high pressurized liquid fuel comes out. At some distance from the nozzle tip, the liquid core breaks up resulting in small droplets which is known as atomization process. These droplets mix with the air in the combustion chamber, increasing their temperature due to the heat transferred from the hot surrounding gases and the droplets start to vaporize. As soon as they reach the ignition point, the mixture starts to burn. This overall process that spans from start of injection to ignition is known as ignition delay.

Ignition first takes place in those areas where the vaporized fuel is properly mixed with air. This is called premixed combustion.

After the premixed phase the temperature rises and more fuel vaporizes, the combustion continues in the flame as far as the fuel meets air to react with. The burning rate is then controlled by the ability of mixing the fuel and air, thus this phase is called mixing controlled phase. Increasing turbulences helps to speed up this stage. The process goes on, until all the fuel has been burnt [13].

2.3.2 NO formation in Diesel sprays

There are mainly three ways of NO formation in combustion namely, thermal NO, prompt NO, fuel NO and NO_2 decomposition.

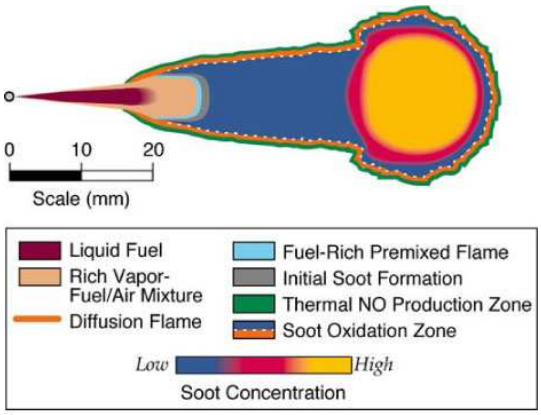

Figure 9. Spatial distribution of thermal NO and soot in a diesel spray. [12]

2.3.2.1 Thermal NO

Thermal mechanism, also known as Zeldovich mechanism, takes place in those zones of the flame where the temperature is high enough to oxidize N_2. This formation process occurs through the next three reactions:

Table 5. Thermal NO reactions and reactions rate constant [13]

Reaction	Reaction rate constant
$O + N_2 \leftrightarrow NO + N$	$k^+ = 7.6 \cdot 10^{13}\, exp(-38000 / T)$
	$k^- = 1.6 \cdot 10^{13}$
$N + O_2 \leftrightarrow NO + O$	$k^+ = 6.4 \cdot 10^{9} T\, exp(-3150 / T)$
	$k^- = 1.5 \cdot 10^{9} T\, exp(-19500 / T)$
$N + OH \leftrightarrow NO + H$	$k^+ = 4.1 \cdot 10^{13}$
	$k^- = 2.0 \cdot 10^{14}\, exp(-23650 / T)$

As can be noticed, the temperature dependence is very high so the formation mainly takes place in the slightly lean regions of the flame where the oxygen concentration is still important.

The first reaction requires a big activation energy, thus it is the one that controls the overall formation. On the other hand the last reaction is not very significant, so that it is usually neglected. Then, the combination of the first and second equations leads to:

$$N_2 + O_2 \Leftrightarrow 2NO \quad (8)$$

and the NO formation rate is given by:

$$\frac{d[NO]}{dt} = \frac{6 \cdot 10^{16}}{T^{1/2}} \exp\left(\frac{-69090}{T}\right)[O_2]_e^{1/2}[N_2]_e \quad (9)$$

It needs to be marked that these concentrations correspond to equilibrium. However, in internal combustion engines (ICE), as the NO formation happens very fast, considerable quantities are frozen during the expansion stroke, when the combustion gases are cooled down.

2.3.2.2 Prompt NO

Also known as Fenimore NO formation. It happens under fuel rich conditions near the flame. In these zones, the intermediate radicals react with N_2 producing amines and cyanocompounds, which are oxidized into NO in the leaner region, through complex reactions [3]. This mechanism is governed by the next reaction stated by Browman and Stone [2]

$$CH + N_2 \rightarrow (HCN_2)^* \rightarrow HCN + N \quad (10)$$

whose formation constant is:

$$k^+ = 4.3 \cdot 10^{12} \exp(-11060 / T) \quad (11)$$

2.3.2.3 Fuel NO

Commercial fuels usually contain species like amines that include nitrogen in their molecular formulas. During the combustion process, this nitrogen can be first discomposed into other intermediates and finally oxidized into nitric oxide.

Efforts to reduce the number of these nitrogenous species are being carried out, for example improving fuel distillation processes.

2.3.2.4 NO_2 decomposition

Interactions between NO_2 and NO have to be taken into account when trying to quantify NO formation. This process is governed by the following reaction:

$$NO + OH_2 \rightarrow NO_2 + OH \quad (12)$$

However, formation of atomic oxygen and hydrogen during the combustion process leads to NO_2 decomposition:

$$NO_2 + O \rightarrow NO + O_2 \quad (13)$$

$$NO_2 + H \rightarrow NO + OH \quad (14)$$

These two reactions are more likely to happen than the previous one leading to bigger amount of NO than NO_2. Thereby, the NO_x emissions during combustion are represented only by NO.

2.3.3 Characteristics of NO formation in DME flames

The main difference between dimethyl ether and other fuels used in Diesel sprays is the presence of C-O bonds instead of C-C bonds. Different researches have been done in comparing the NO formation between DME and regular Diesel in engines.

D. Cipolat compared the NO emissions in a Diesel engine at a range of speeds comparing DME with regular fuel keeping the same operating conditions. DME showed bigger emission rates at low speeds and almost equal at medium and high speeds. High injection pressures resulted in small droplets which vaporized very fast, leading to high NO formation rate, especially in DME. The lower equivalence ratio when fuelling with DME led to lean mixtures, thus increasing Zeldovich NO [15].

Other researchers (Zhen Huang *et al*) have shown that NO emissions can be reduced for DME in a given engine it the operating conditions (injection timing...) are optimized to run with DME. Moreover, the performance of the engine was kept the same. EGR was reported as a great contributor in NO reduction [20].

Finally, Chang-Eon Lee compared NO formation in a non premixed flame, using DME and an ethane/oxygen mixture containing the same C, O, H composition as DME, in order to quantify the importance of the C-O bond. It was found that the major production path (Figure 10) of NO was:

$$N_2 \rightarrow HCN \rightarrow COH \rightarrow N \rightarrow NO \quad (15)$$

This reaction was believed to happen through complex interactions between thermal and prompt mechanisms. However these reactions are reduced due to partial burning characteristics of DME and other NO reactions which are activated by the C-O bond [14]. The main formation paths are shown in Figure 10:

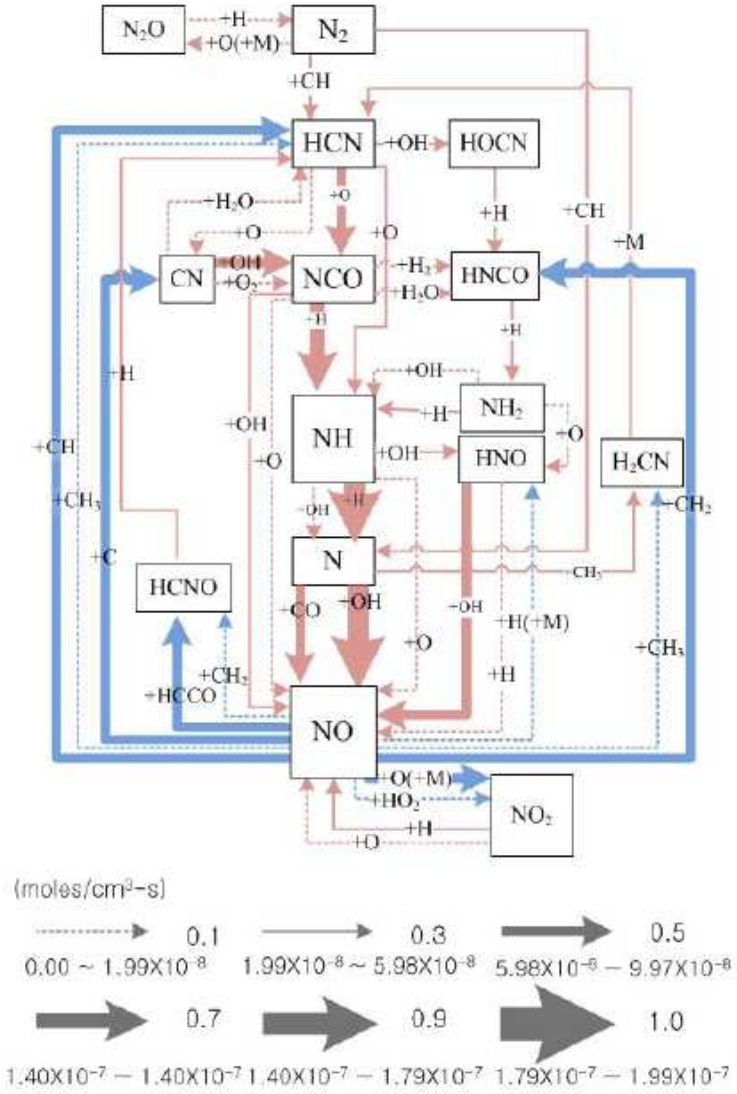

Figure 10. Paths of NO formation in DME combustion. [14]

3 Experimental methodology

3.1 Experimental set-up

3.1.1 Equipment

The equipment used in the experiments is described in the next paragraph:

Cell G

The experiments have been performed in a high pressure combustion chamber (Cell G) which is provided of several quartz windows to visualize the sprays inside. The quartz windows have a good light transmittance for a wide range of wavelengths. It can withstand pressures up to 100 bar and temperatures up to 650ºC. The air flow is provided by a compressor and three heaters (two air heaters and a surfaces heater) regulate the air temperature. It is cooled by a water flow pressurize at 2-3 bar. The inner dimensions are 100mm diameter by 150 mm height.

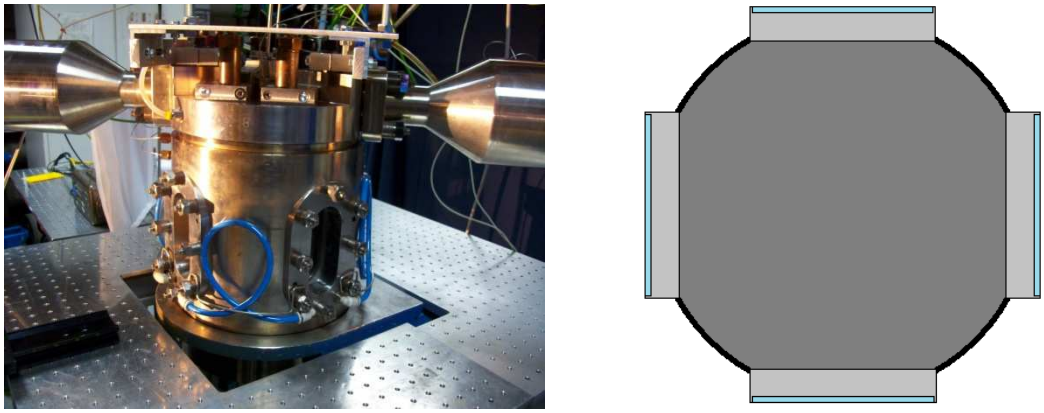

Figure 11. Combustion chamber.

The cell is used in its four window configuration as it can be seen in Figure 11.

DME injector

The injector used is a Volvo-Delphi DME common rail injector for heavy duty engines. It was used in it single orifice configuration. It is connected to a high pressure pump that provides injection pressures about 360 bar.

The injector is connected to a high pressurized common rail. This pressure is supplied by a DME pump connected to the common rail with several hoses.

Figure 12. DME injector.

Laser

The laser source consists of a dye laser manufactured by Quantel International fed with Rhodamine 590, suitable for the operation range as it can be seen in the Figure 13:

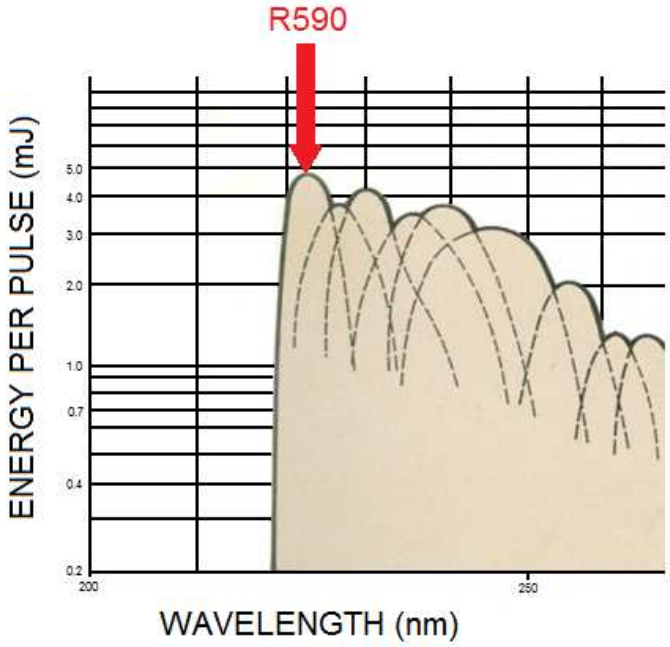

Figure 13. Laser intensity distribution for different dyes and wavelengths.

In order to get a more stable range, it was thought to add small amounts of Rhodamine 610.

This dye laser is pumped by a Nd:YAG laser. Nd:YAG laser is supplied by a flash lamp, accomplishing an output wavelength of 1064 nm. Some of this light is doubled in a crystal arrangement, achieving wavelengths around 532 nm. These two beams (infrared and green) are led into the dye laser.

The green light is led into a dye cell (oscillator) which is connected to a tunable grating. The tunable grating can be leant providing a range of wavelengths: around 552-584 nm when using Rhodamine 590 as a dye. Then, the light beam passes through a preamplifier and an amplifier (dye cells) pumped by the green light beam, where the power is greatly increased.

In a final stage, this wavelength is doubled (in a DCC-3 crystal) getting wavelengths about 267-295 nm. This beam is mixed (in a MCC-3 crystal) right after with the infrared light from the Nd:YAG achieving a final wavelength about 217-245 nm.

However, in order to obtain as much energy as possible the green light has to be delayed through some internal reflections. The aim of doing so is to get phase matching between both light beams, increasing the efficiency of the mixing crystal. There are several layouts for the delay path. In the current experiment, the delay path is not optimized for the output wavelength but it is used because of its simplicity.

Figure 14. Dye laser Stage 1: oscillator and amplificator.

Intensified charge-coupled device (ICCD) camera

The visualization of fluorescence is performed by two recording cameras (LaVision DynaMight). Each one is equipped with a CCD sensor with 1024 x 1024 pixels. The CCD sensor emits one electron when receiving a photon, for further readout and digitalization. However the electric signal has a low power and it needs to be intensified in an amplifier.

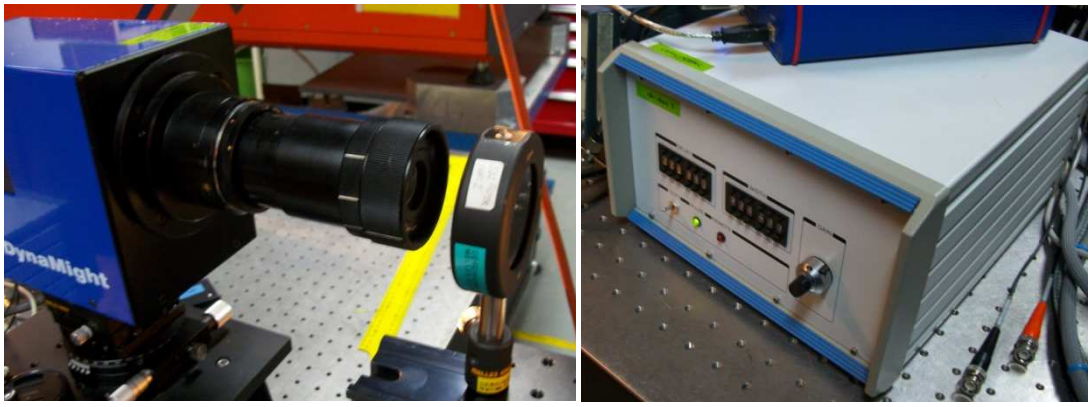

Figure 15. CCD camera (left) and intensifier (right).

In order to cut off the scattered light (and the emission at different wavelengths if necessary), bandpass filters are attached to the lens. The filter is attached to the lens of the camera as it can be seen in the picture above.

High speed camera

In order to visualize the spray atomization and flame development a high speed camera is used in a former experiment without laser illumination. The camera used is a Phantom Digital High Speed camera v7.3. It has a resolution of 800x600 and captures 222.222 frames per second. The images are black and white.

Figure 16. High speed video camera.

3.1.2 Experiment layout

3.1.2.1 Expreriment 1: fluorescence detection

A top view of the experiment devices is shown in Figure 17:

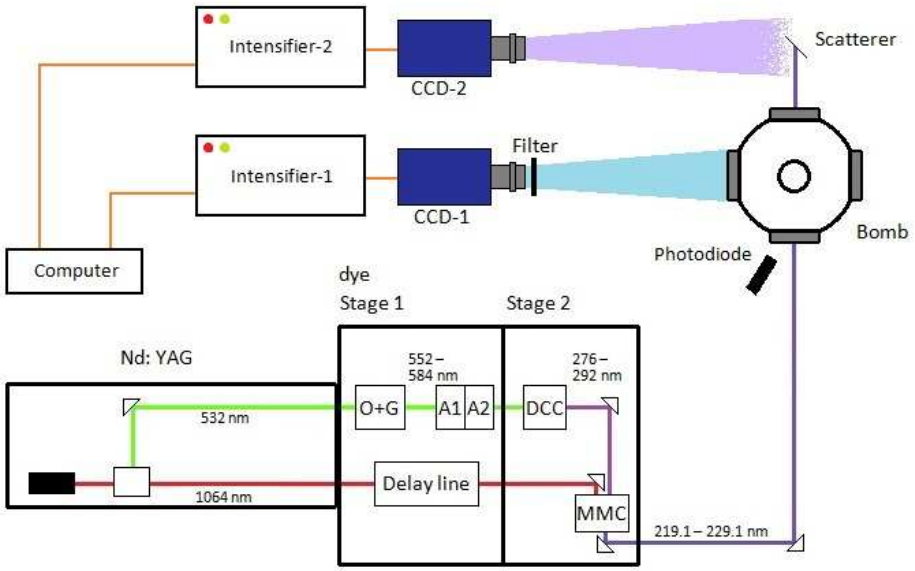

Figure 17. Experiment 1 top view.

The laser source emits the light beam. By using a prism the beam is deflected 90º and redirected into the chamber. It travels through the flame and when it goes out it is scattered by a tilted mirror. CCD camera 1 (CCD-1) has a filter attached and it detects images the fluorescence when receiving a signal, whereas CCD camera 2 (CCD-2) detects the laser beam shape to know its distribution and the attenuation along the chamber. Both images are intensified and displayed in a computer.

3.1.2.2 Experiment 2: spray visualization

The layout of the spray visualization experiment can be seen in Figure 18:

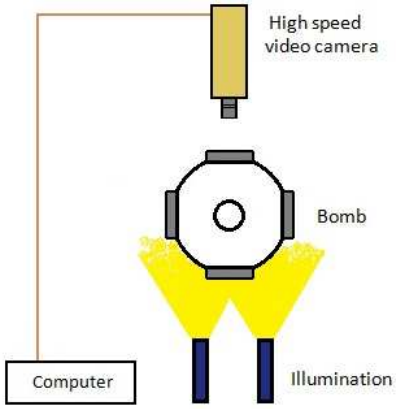

Figure 18. Experiment 2 top view.

The spray is illuminated on one side by two light sources. The high speed video camera is placed on the opposite side of the chamber capturing images of the spray and showing them in the computer. Images of the flame luminosity are also captured with the same arrangement, but switching of the lamps.

3.1.3 Equipment synchronization

It was necessary to synchronize the laser, the injection event and the ICCD camera. This is done by triggering the laser pulse and the ICCD camera with the logical signal to the injector. In order to take pictures at different times after the start of injection, the laser pulse and the camera were delayed in respect to this logical signal.

Due to the long time to read out the data from the ICCD device, it is not possible to take more than one picture per injection. Thus, an image is taken every 10 s, which is the time between two consecutive injections.

3.2 Calibration

3.2.1 Laser frequency and irradiance

As it has been reported earlier, it was necessary to tune the laser beam to wavelengths around 226 nm, in order to excite the NO A←X (0, 0) bands. Since no wavemeter was available to adjust the laser, the calibration was done by an arrangement consisting of a photomultiplier, a monochromator, a detection sensor and an oscilloscope.

First, the monochromator had to be calibrated by using an UV lamp whose spectrum was known. By tuning the scale in the monochromator, the oscilloscope showed that the peak at 253.65 nm in the UV lamp matched 265.65 on the display. Hence, a constant offset of 12.00 nm was assumed for the device, regardless the wavelength.

After this, a low power laser beam was led into a rough mirror to induce its dispersion. Some of this scattered light was captured by the photomultiplier and monochromator. By adjusting the grating manually, the wavelength could be switched to different values in short steps. The angles of the frequency mixing and doubling crystals were modified at the same time. A wavelength of 226 nm (238 nm on the display) was finally achieved.

Nevertheless, in NO excitation a finer tuning is necessary, so that the laser beam frequency matches one strong rotational transition in the NO spectrum. In order to get a more specific wavelength the arrangement in Figure 19 was used.

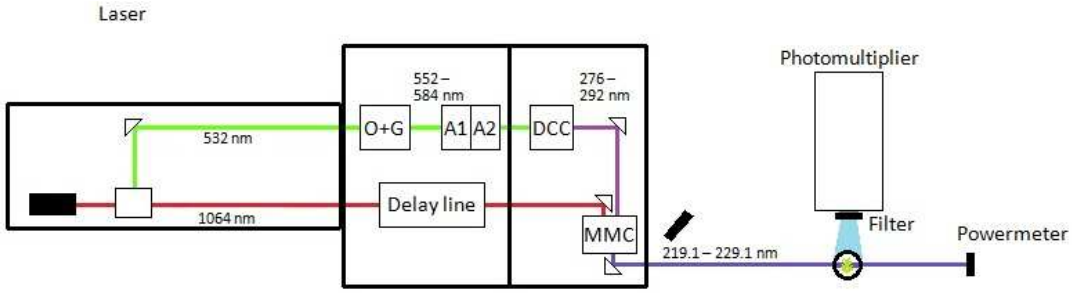

Figure 19. Top view of the wavelength tuning layout.

The laser beam was directed into a gas cell containing N_2 seeded with 300 ppm of NO and pressurized at 2 bar. The fluorescence was filtered and the signal was collected by the photomultiplier and the power of the outgoing laser beam was measured in a powermeter. Then, those steps where the relation between the signal from the photomultiplier and the powermeter is higher correspond to the peaks in the spectrum (high fluorescence and low power due to the absorption).

However, when optimizing the wavelength to get the best signal, there are other two facts that have to be considered.

First, the laser, according to Figure 13 does not emit at the same power for every wavelength. Since at higher pressures the attenuation is much stronger, it is necessary to keep the power as high as possible.

Second, small changes in the temperature of the crystals inside the laser device can vary the output wavelength. Due to this fact, it is advisable to match a relatively stable peak. Besides, the NO spectra at the cell conditions and the bomb conditions are different and the peaks broaden out and get uniform (and of course reduced), so that getting the wavelength corresponding strongest peak in the cell is not that critical:

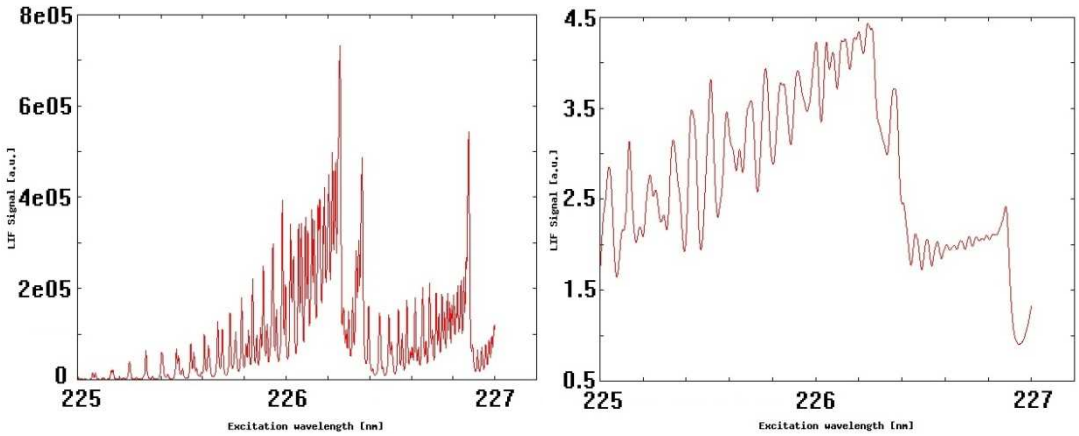

Figure 20. NO excitation spectrum at 2 bar, 300 K and N_2 atmosphere (left) and at 50 bar, 2300 K and air atmosphere (right) simulated with LIFSIM, a LIF spectra simulation tool that uses three-level non-transient linear models and spectroscopic data [16].

Finally, although in the current experiment it was not possible since no wavemeter was available, O_2 interference has to be taken into account. Oxygen Schumann-Runge excitation bands overlap the A←X (0, 0) bands as it can be seen in the next figure:

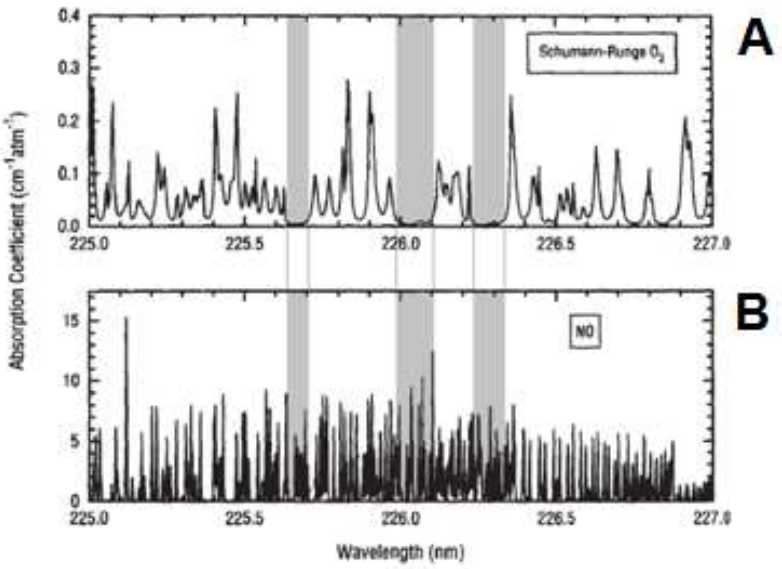

Figure 21. O_2 Schumann-Runge excitation bands (A) and NO (0 , 0) excitation bands (B) [17].

So the excitation wavelength must reduce the O_2 interference as much as possible in order to have accurate measurements. In the current experiments O_2 is a source of error hard to quantify.

3.2.2 Optics selection

First, using LIFSIM software a simulation of the emission spectrum was carried out, setting similar conditions expected in the flame (50 bar; 2000 K).

The filter selection was performed according to Figure 8. An ideal filter should have no transmittance at the laser wavelength (226 nm) and 100% transmittance at the fluorescence wavelength.

Sine no ideal filters exist, filters with a center wavelength of 248 nm and 254 nm were considered. Furthermore, a UG5 (Appendix) filter was available as well. In order to achieve the wavelength vs. transmittance graphics of the filters (not provided) a spectrometer was used. A sweep was carried out and the intensity was measured at each wavelength. The background light was subtracted and the transmittance was calculated using Eq. 16:

$$Tr = \frac{I_{filtered} - I_{background}}{I_{not\_filtered} - I_{background}} \quad (16)$$

The graphics are shown in Figure 22:

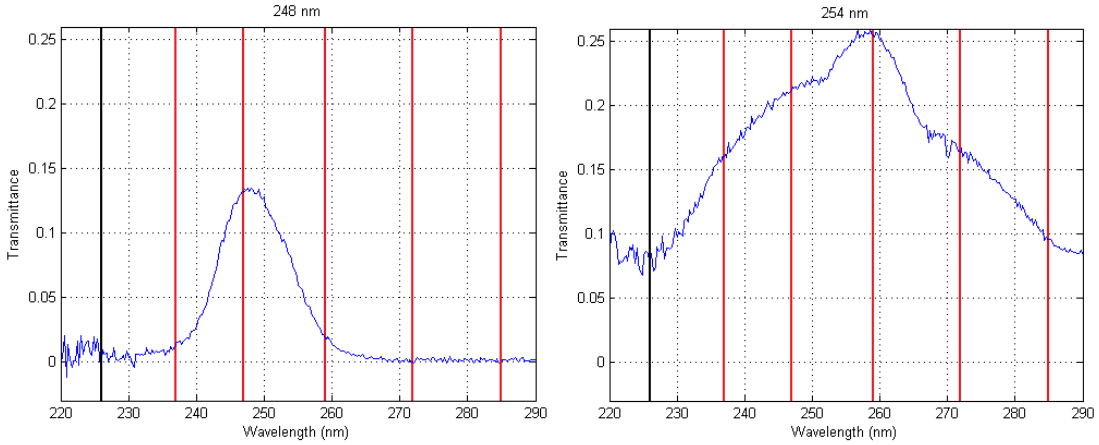

Figure 22. Transmittance of the 248 nm filter (left) and 254 nm filter (right). Scattered light (0, 0) marked in black and (0, 1), (0, 2), (0, 3), (0, 4) and (0, 5) transitions, in red (from the left to the right).

As it can be seen the 248 nm filter blocks much more efficiently the scattered light, it transmits the fluorescence worse though. It can also be noticed that at short wavelengths the signal is very noisy since the spectrometer signal was too low. Combinations of these filters with the UG5 were also tested:

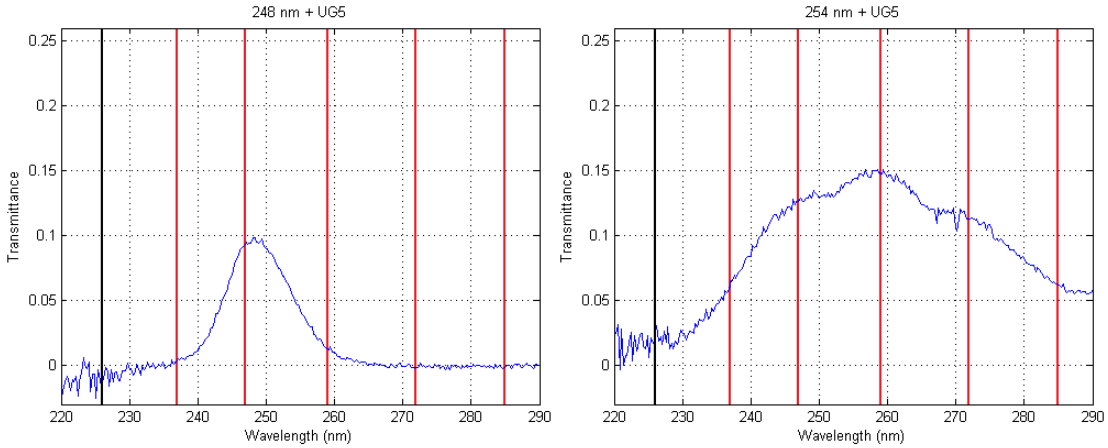

Figure 23. Transmittance of the 248 nm filter combined with the UG5 (left) and 254 nm filter combined with the UG5 (right). Scattered light (0, 0) marked in black and (0, 1), (0, 2), (0, 3), (0, 4) and (0, 5) transitions, in red (from the left to the right).

All the combinations, except the 248 nm + UG5, seemed to transmit some scattered light, so that combination was chosen for the experiments. The detection will take place mainly in the A→X (0, 2) band (T ~ 10%) and the A→X (0, 3) band (T ~ 1.5%), which have strong enough emissivity (Figure 23 left).

The quartz windows of the chamber were tested as well in order to ensure that they do not attenuate the signal so much. All showed a transmittance of 80% at 200 nm – 300 nm.

3.3 Measurements

3.3.1 Performance

In order to get a good understanding about how NO is formed in DME flames, measurements were taken with different configurations. The laser beam path was moved from 10 mm below the injector nozzle tip, up to 90 mm below the tip in steps of 20 mm, in order to have spatial information about the nitric oxide formation.

Then, measurements were taken at different times after the start of injection. Starting at 3 ms aSOI and delaying it in steps of 1-2 ms. The logical injection duration for all the measurements was set to 15 CAD at 1200 rpm (approximately 2.1ms).

The conditions in the chamber were kept the same for all the measurements, working with an injection pressure of 300 bar, a chamber pressure of 50 bar, a temperature of 560-570ºC and a constant air flow of 15-17 l/s.

Finally another set of measurements was taken at 90 mm below the nozzle but with an increased injection pressure of 360 bar, in order to understand the NO formation dependence with injection pressure.

Ten images were taken in each measuring point. The next matrix gathers all the points.

Table 6. Experiment matrix. Each cell shows the injection pressure in MPa. ND: No Data

		Time aSOI [ms]										
		3	4	5	6	7	8	9	10	12	14	16
Distance from the nozzle tip [mm]	10	*30*	*30*	*30*	*30*	*30*	*30*	*30*	*30*	*30*	*30*	*ND*
	30	*30*	*30*	*30*	*30*	*30*	*30*	*30*	*30*	*30*	*30*	*ND*
	50	*30*	*30*	*30*	*30*	*30*	*30*	*30*	*30*	*30*	*30*	*ND*
	70	*30*	*30*	*30*	*30*	*30*	*30*	*30*	*30*	*30*	*30*	*ND*
	90	*30*	*30*	*30*	*30*	*30*	*30*	*30*	*30*	*30*	*30*	*ND*
	90	*36*	*36*	*ND*	*36*	*ND*	*36*	*ND*	*36*	*ND*	*36*	*36*

Background images without any flame were taken as well in order to reduce the noise and scattered light coming from reflections of the laser beam inside the chamber.

3.3.2 Post processing

The sets of ten pictures from both cameras were averaged and the mean background was subtracted. Afterwards, the averaged images were trimmed in order to keep only the part where the excitation and fluorescence take place to minimize the computational time.

In order remove the scattered light from the laser and have smoother images, filtering was carried out in images from CCD–1. The filter consisted of a weighted average in every pixel using the pixels placed in an *x*-pixel radius circle centered in the initial pixel. The radius of this circle (*x*), in other words the strength of the filter, was set intending to reduce the noise as much as possible while keeping the initial distribution in the picture.

Once the images were filtered, the next step consisted of a vertical integration of the fluorescence. This way it was possible to know the variation in fluorescence along the flame (along the beam path).

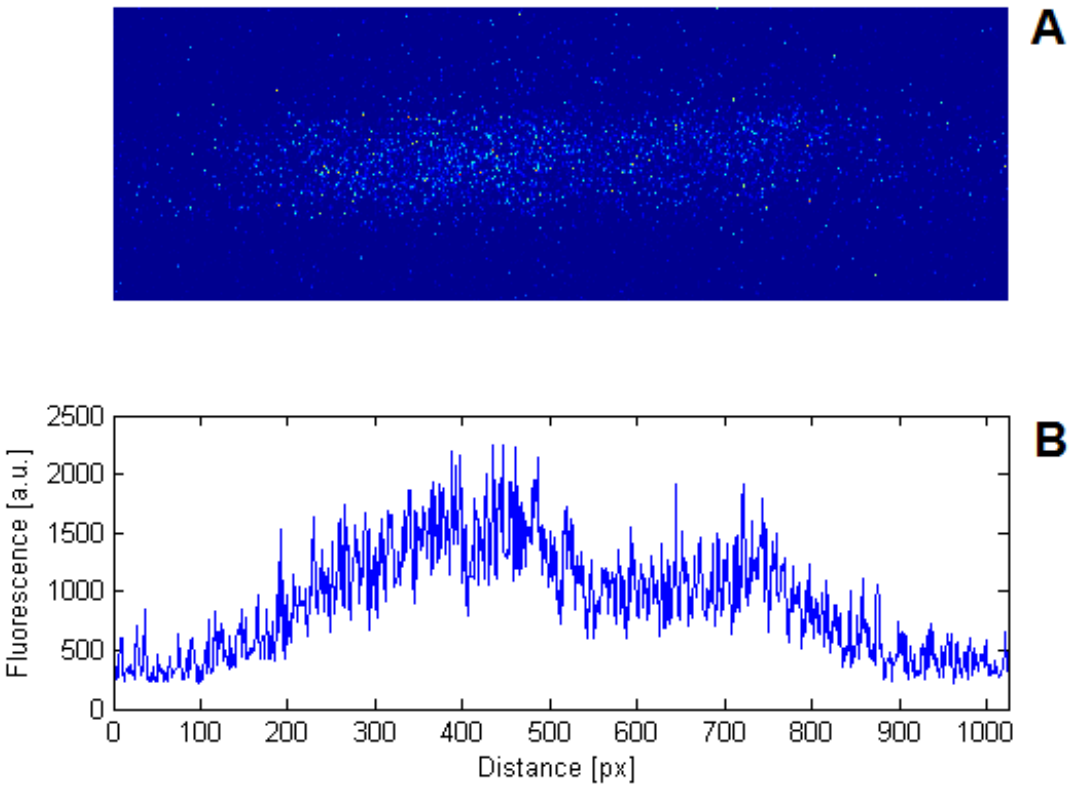

Figure 24. Image from the CCD-1 camera (A) and spatial integration (B) without filtering. The point corresponds to the average at 50 mm from the nozzle, 8 ms aSOI at 300 bar. 10 mm = 193 pixels.

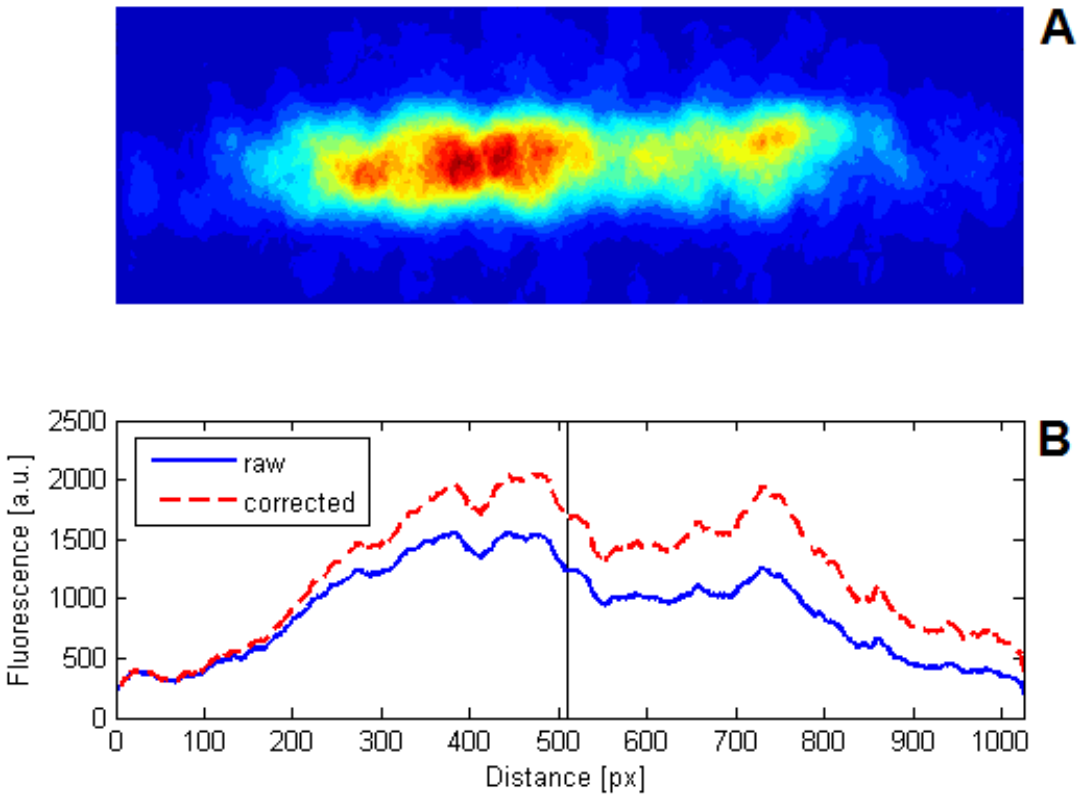

Figure 25. Filtered image from the CCD-1 camera (A), spatial integration of the fluorescence without correction (B, blue curve) and corrected (B, red curve). The point corresponds to the average at 50 mm from the nozzle, 8 ms aSOI at 300 bar. 10 mm = 193 pixels. The black line shows the center line of the nozzle.

The standard deviation of every set of 10 images was calculated for the integrated images.

A change in the scale was also made in order to convert the pixels into dimensions. To do that a grid was introduced inside the chamber and images were taken, correlating pixels and dimensions. The relation turned out to be 10 mm = 193 pixels. The new scale was introduced in graphics, setting the center line of the nozzle orifice as reference (0).

Since the fluorescence is proportional to the intensity of the laser beam and this suffers a big attenuation during its way through the chamber, a correction for the attenuation was introduced. This was done using Lambert – Beer's law:

$$I = I_0 \cdot e^{-\sigma N x} \quad (17)$$

Lambert – Beer's model was developed for homogeneous environment. However, despite the flame is a highly heterogeneous environment, this model was used because of its simplicity. The σN parameter was adjusted having in mind that in an ideal case the distribution must be symmetrical. The result can be seen in Figure 25 (red curve).

Nevertheless, this coefficient is temperature dependence, which means that a correction that could work well for a measurement at a given time could not be good at a different time. The σN parameter was then chosen to give a good correction in most of the measurements.

The total fluorescence for each measurement was then integrated obtaining plots for the NO fluorescence variation with time aSOI at every relative position from the nozzle. The same was done for the measurements at the two different injection pressures.

Regarding the images from camera CCD–2, no filtering was carried out. The intensity of the beam was integrated to verify that the laser beam profile did not show any irregularity. This information can be used for attenuation correction models.

4 Results and discussion

4.1 Spatial-time distributions

The variation of the NO fluorescence for different times aSOI at all the positions measured is shown in Figure 26:

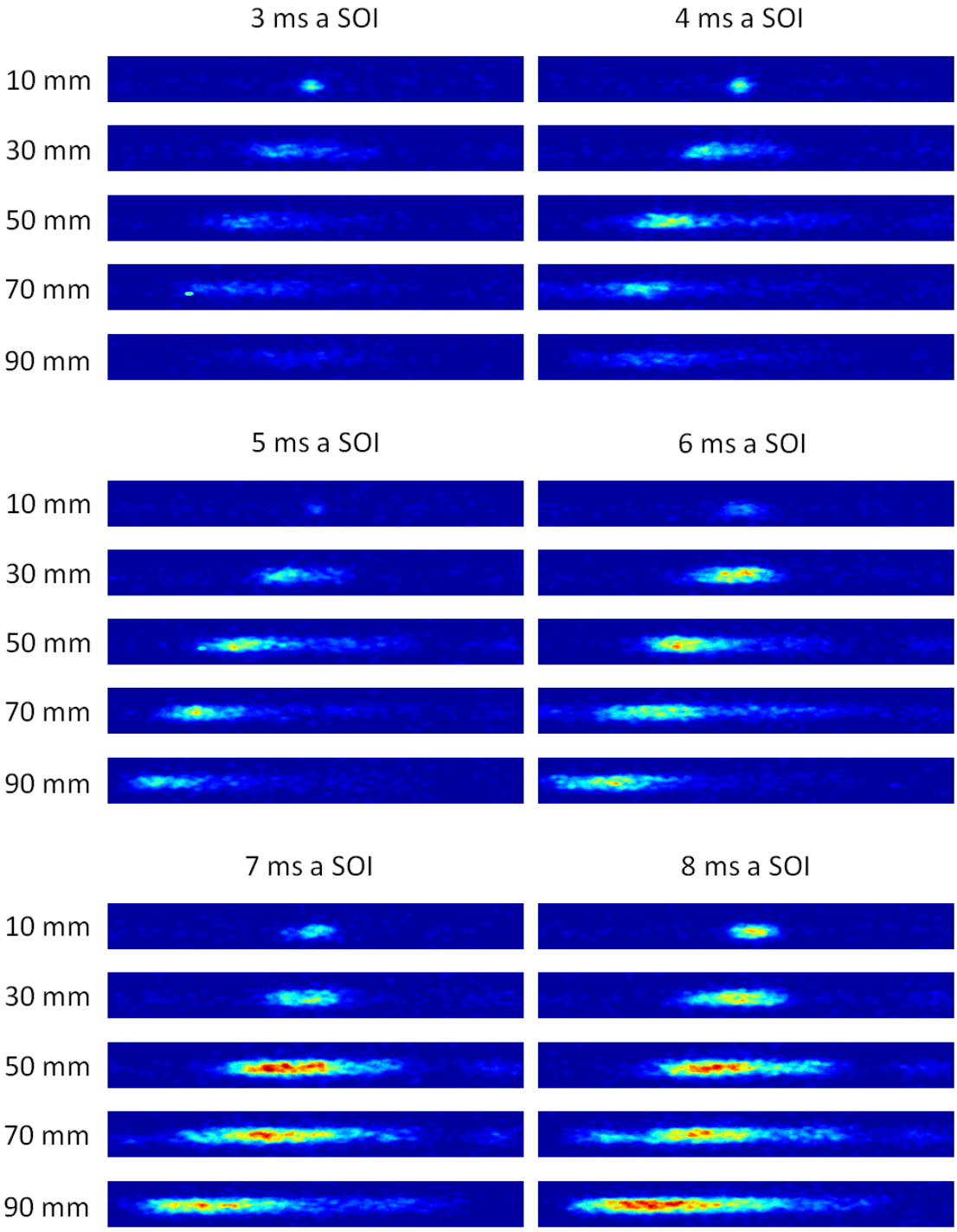

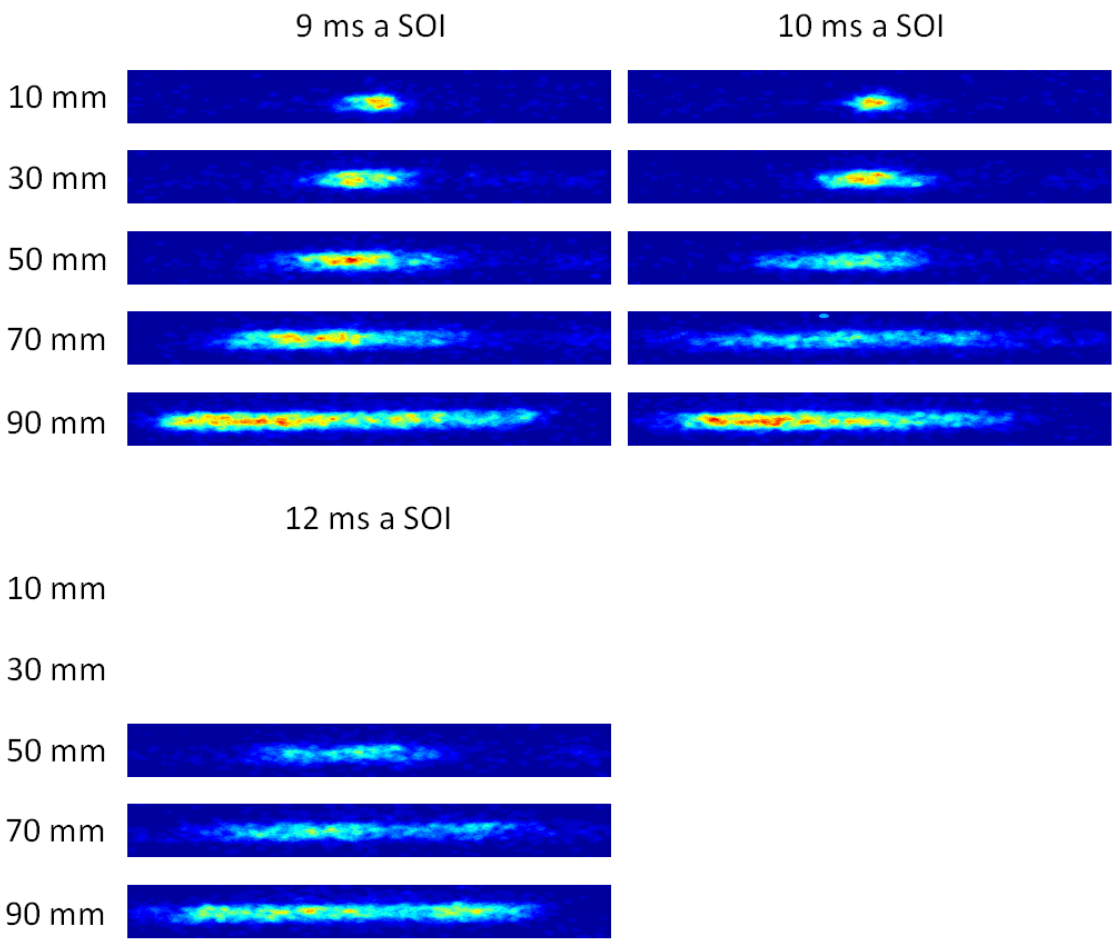

Figure 26. NO fluorescence in filtered images at every measured point for an injection pressure of 300 bar.

The graphics of the integrated and integrated and corrected NO fluorescence give a better understanding about the NO formation and it is shown in Figure 27:

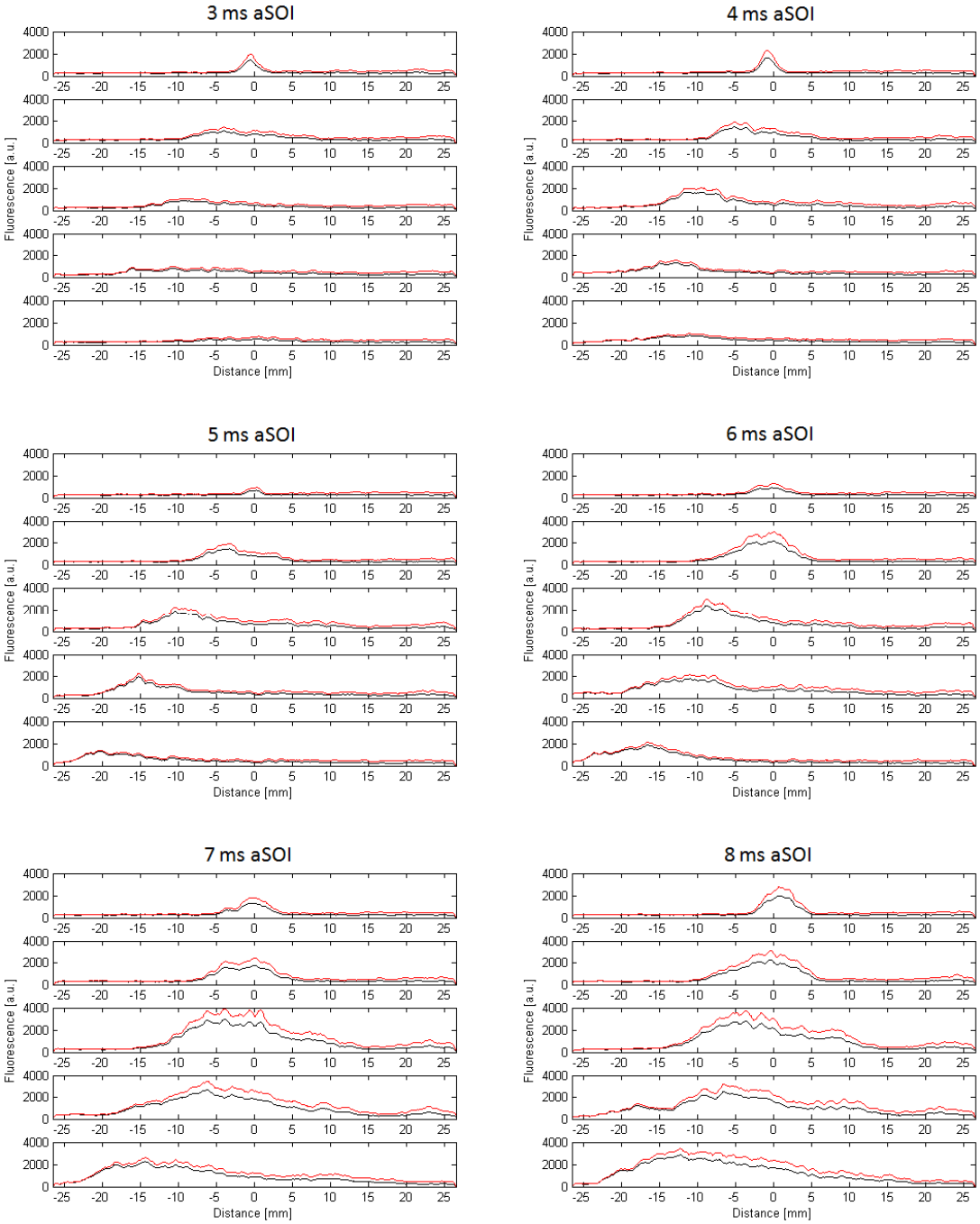

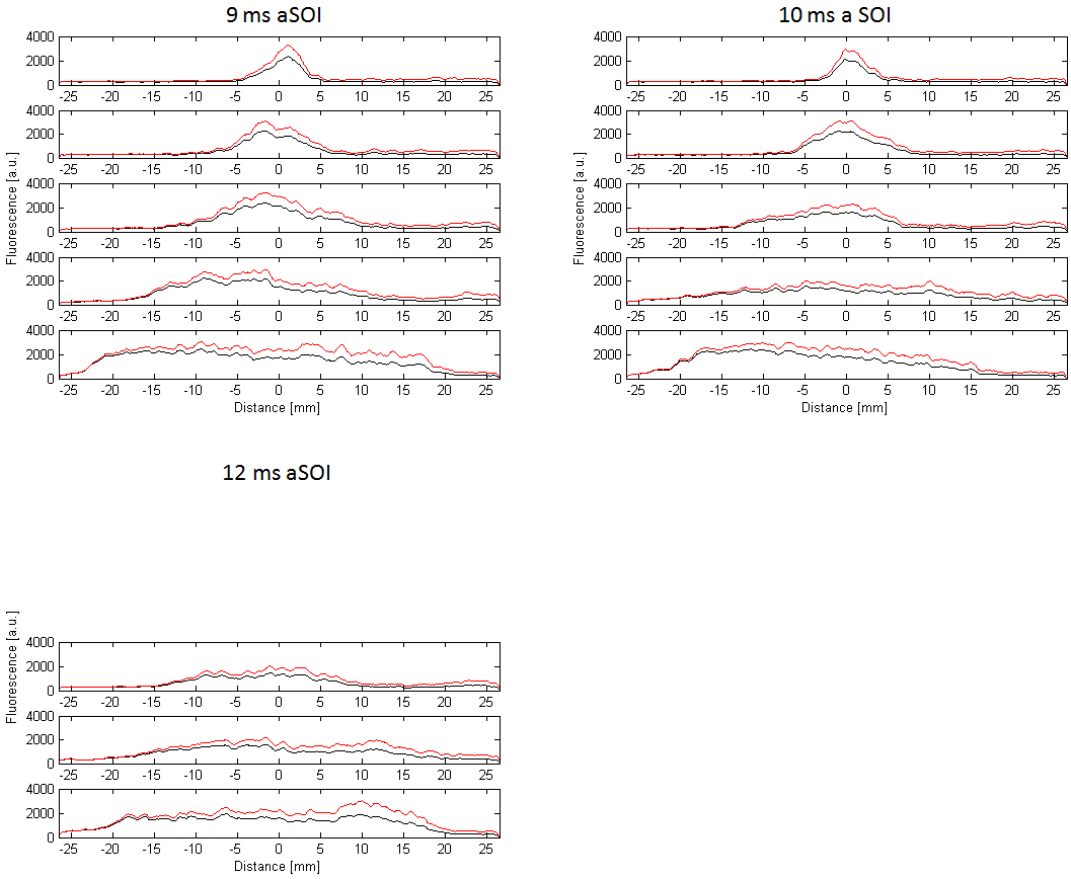

Figure 27. Vertical integration of the fluorescence of the images in Figure 24. Black line represents non-corrected data. Red line represent corrected data.

Most of the integrated graphics, especially after 7 ms aSOI, show two peaks almost equally distanced from the nozzle center line. These two peaks correspond with the areas where the nitric oxide is mainly formed, which are the contours of the DME flame plume. In these areas there are two facts that contribute to the nitric oxide formation via the thermal mechanism: on one hand the temperature is high and on the other, the concentrations of nitrogen (from the air) and oxygen (both from the air and from the fuel) are high. The feature that the left peak is much stronger than the right one relies on the fact that the laser beam travels from the left to the right side. Some of the laser intensity is absorbed by the NO, and some is just attenuated by the gases at high pressure, mainly hot CO_2, intermediate species and probably DME. Thereby, when the light beam reaches the right contour of the flame the excitation is much lower, thus generating less fluorescence, and that the second cannot be distinguished in some cases. A good model for correcting attenuation must "lift up" this peak, making it equal on the left and right hand side and resulting in a symmetrical fluorescence distribution.

The fact that the DME molecule contains atomic oxygen, contributes not only to reduce soot and therefore attenuation, but also seems to make the NO formation more uniform than in other fuels [2]. This oxygen may be involved not only in the regular combustion process, but also in thermal NO reactions when meeting N_2 molecules (Table 5: reaction 1).

The images show that most of the NO is formed 7 ms aSOI and at distances relatively far from the nozzle. After 9 ms aSOI, it can be seen that the NO distribution starts to be more uniform, which can be due to molecular diffusion phenomena. NO

concentration drops later (dissociation) due to the decrease in temperature. Nevertheless, an important amount remains. This can be seen in Figure 28, which shows the overall integrated fluorescence:

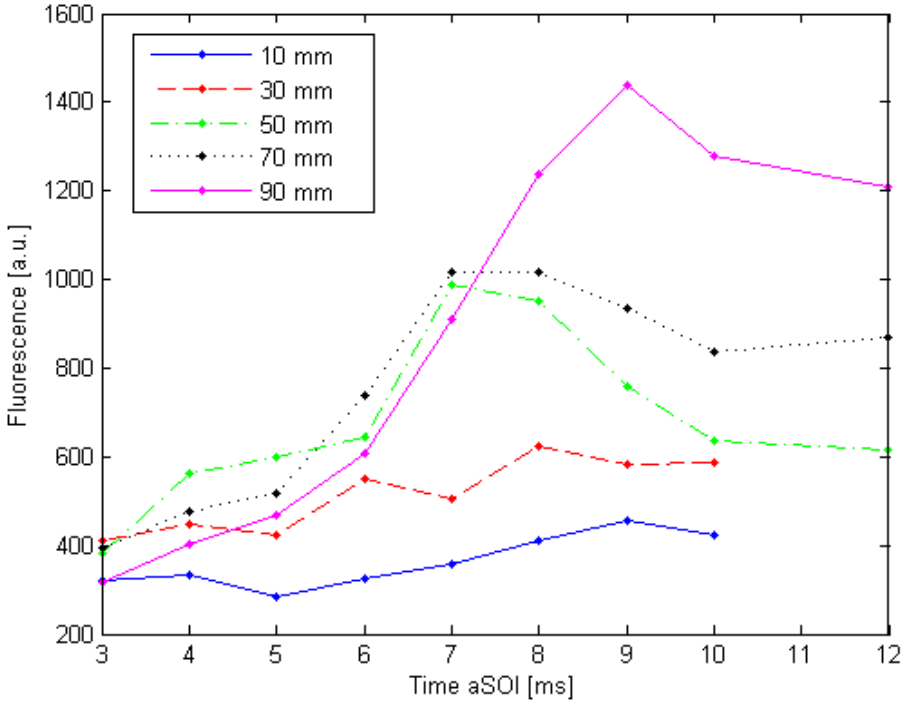

Figure 28. Total integrated fluorescence for every measured point at P_{inj}=300 bar.

According to Figure 28 above, the further from the nozzle the bigger the peak is, because at these distances the initial fuel droplets are smaller, allowing good air entrainment and leading to a rapid fuel vaporization and mixing with air. These facts make combustion to happen faster in these areas, increasing gases temperature and making easier thermal NO formation.

Besides, combustion occurs during a longer time in these areas, so that O_2 and N_2 have enough time to react.

After the point of maximum NO fluorescence, the concentration decays, reaching a constant value, as it was reported before. The fact that an important concentration of NO (frozen NO) remains after the combustion has finished is the reason why NO emissions must be reduced. This frozen NO is expelled though the exhaust system of an engine or burner to the atmosphere, unless it is previously reduced into N_2.

Images from the high speed video camera help to analyze how the formation occurs within flame development:

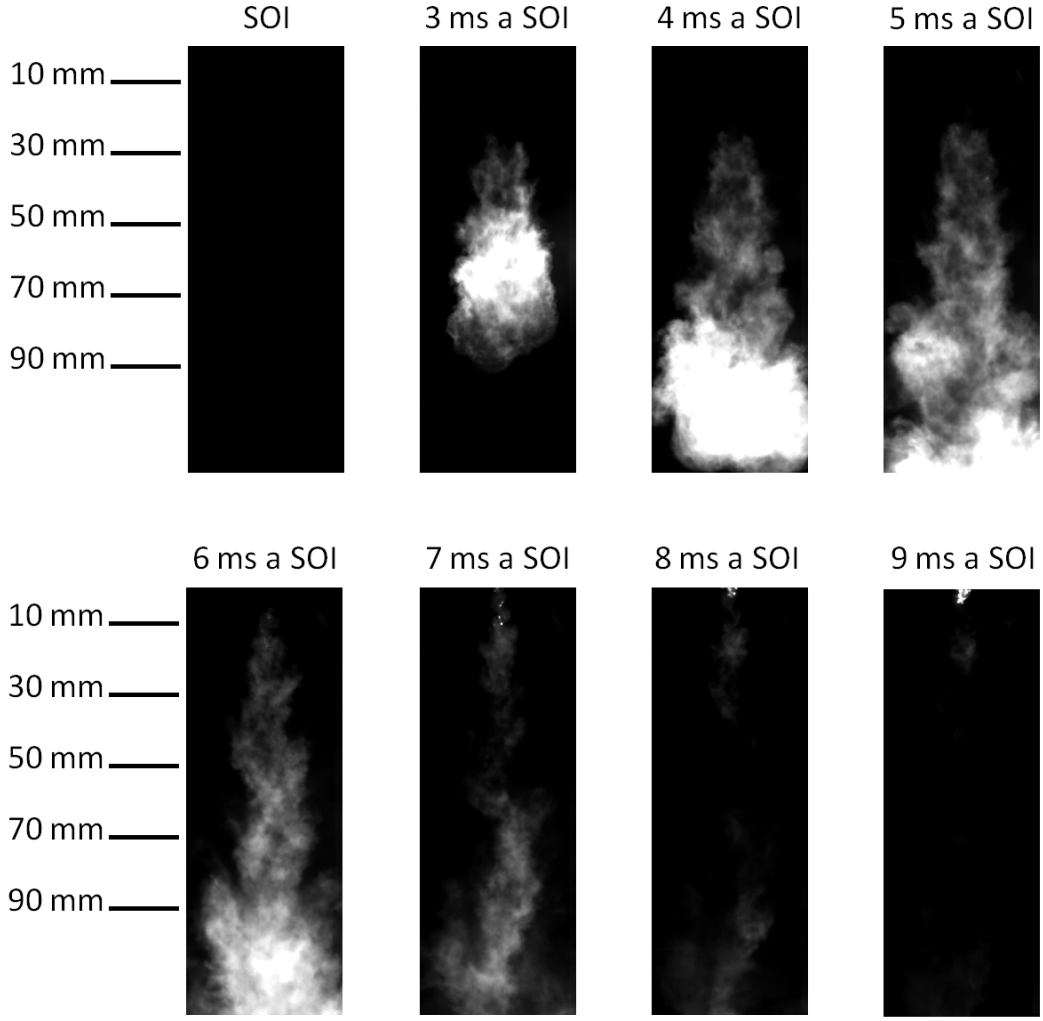

Figure 29. Images from the flame taken by the high speed video camera.

The NO formation rate becomes maximum between 6 ms and 7 ms. As it can be noticed, the combustion has moved on at that time and the temperature is maximum.

Another significant fact is that the laser beam placed at 10 mm does not hit the flame until 6 ms aSOI, and a peak is observed in the integrated measurements at very early times. This may correspond to scattered light from the laser hitting the liquid core, since the combustion has ton started. However, the peak appears again later in the combustion, this time the light is fluorescence from NO since the beam is passing through the now developed flame. The laser beam placed at 90 mm does not cross through the flame either, before 3 ms aSOI. The integrated laser luminosity helps to explain these facts:

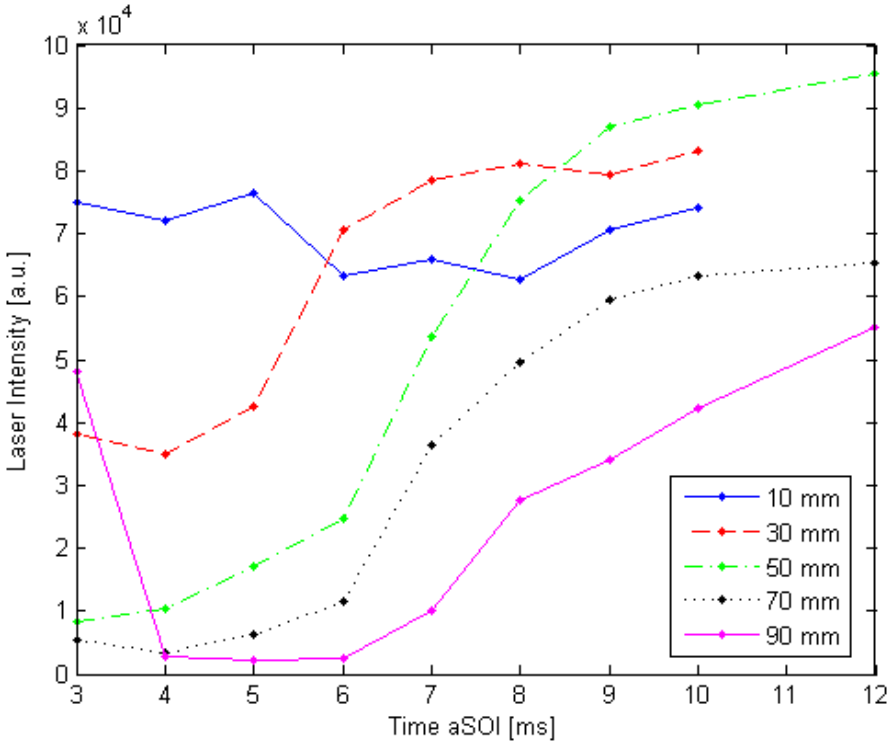

Figure 30. Integrated laser intensity from CCD–2.

Since the laser is not passing through the flame at 3 ms at 90 mm, the attenuation is low and a high intensity comes out. In the beginning most of the curves are relatively flat, and at a later time (5-6 ms), the intensity goes up. This could be caused by a drop in the formed CO_2 temperature and the extinction of some attenuating intermediates.

Figure 30 is a good starting point to develop attenuation models that would provide more accurate results.

4.2 Rail pressure comparison

The NO fluorescence variation within time for two different rail pressures is shown in the following set of images:

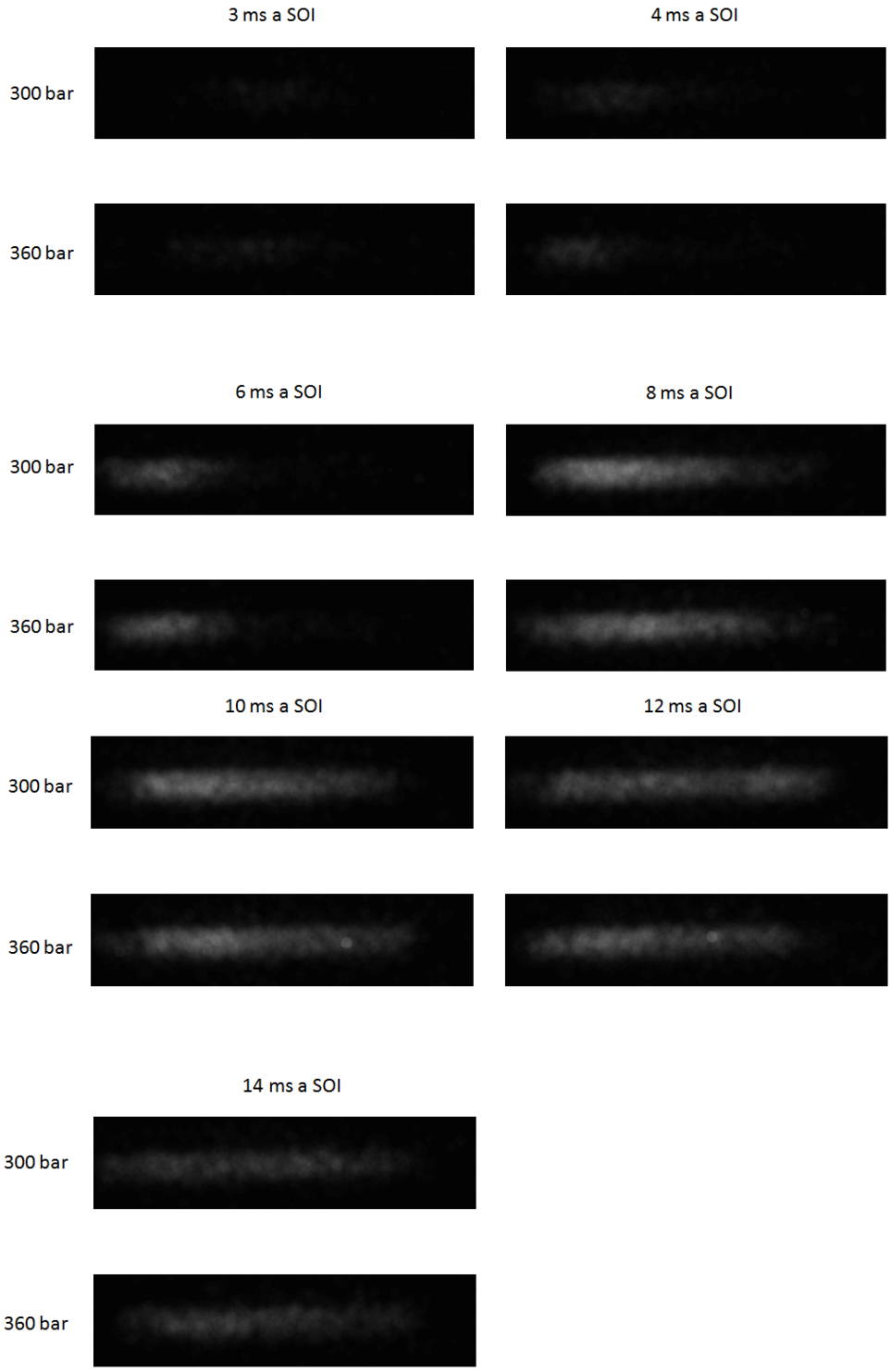

Figure 31. NO fluorescence at 90 mm below the nozzle for 300 bar and 360 bar injection pressures.

The integrated fluorescence is shown in Figure 32:

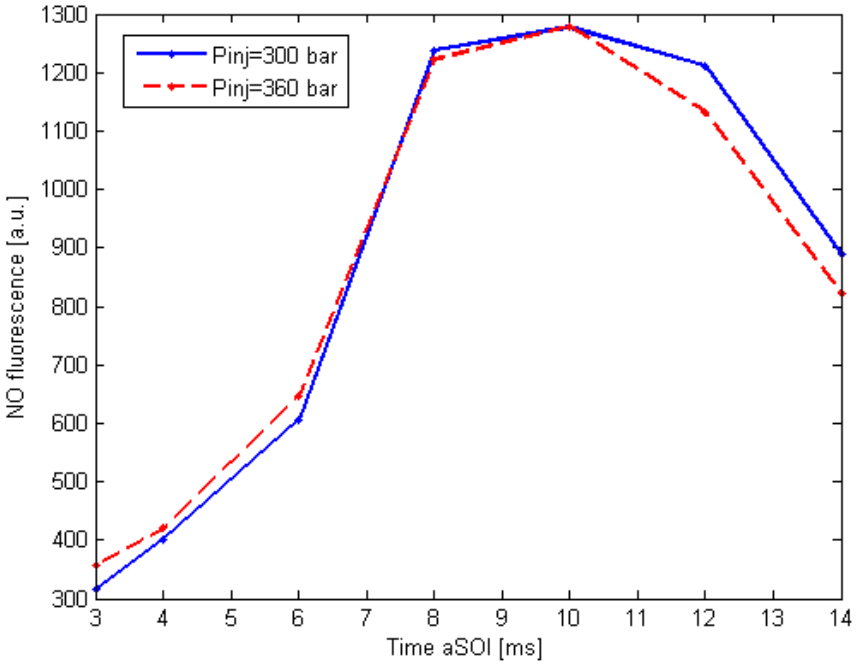

Figure 32. Total integrated fluorescence at P_{inj}=300 bar and P_{inj}=360 bar. Distance from the nozzle: 90 mm.

As can be seen, increasing the injection pressure does not have a significant effect at early times. At late times, increasing the injection pressure results in a decrease in NO formation in respect to a lower injection pressure. Besides during the high pressure experiments one of the windows cracked and the upper part fell interfering the laser beam path. This would have led to a bigger intensity loss so that the difference between the red and blue curves might be larger.

This behavior contradicts previous experiments with different fuels, showing higher NO fluorescence when increasing injection pressure [2,18].

However, from this data, it cannot be concluded that increasing the injection pressure will result in smaller amounts of NO formed, since only NO formation at one distance is being considered. Fuel penetration and plume position could have been modified as well due to the larger differential pressure (see Figure 33). Some zones in the bottom of the chamber (lower than 90 mm from the nozzle) that did not reach the conditions for NO formation, may reach them now. More measuring points are necessary to draw conclusions.

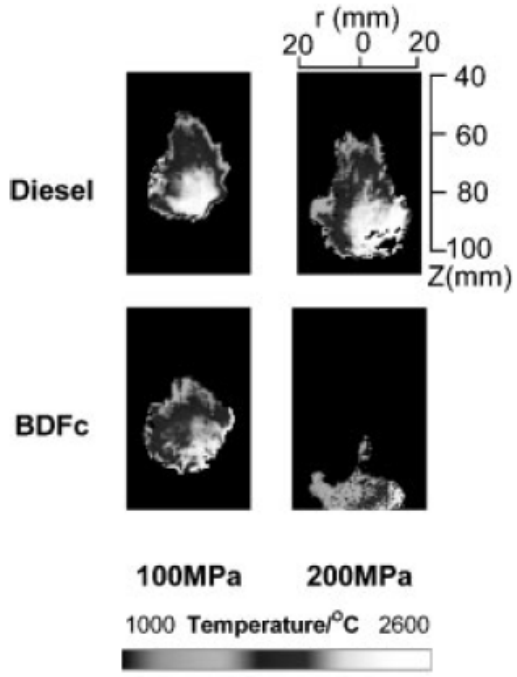

Figure 33. Temperature distribution at 1.6 ms aSOI in a Diesel and a BDFc (biodiesel from cooking oil) flame at two different injection pressures [19].

On the other hand, the standard deviation can be seen in Figure 34. All measurements show an important uncertainty, which means that no conclusions can be drawn about the effect of increasing the injection pressure 6 MPa.

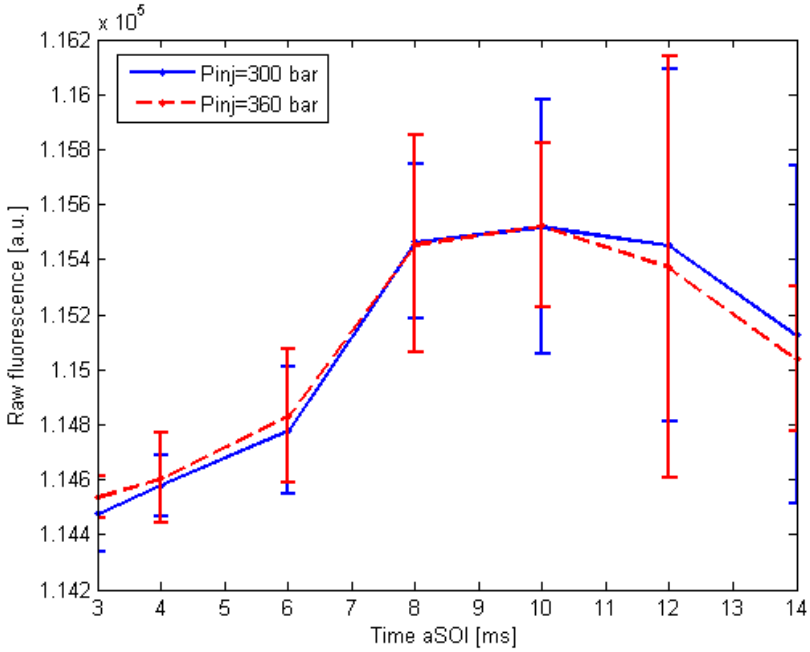

Figure 34. Integrated raw fluorescence and deviation from CCD camera 2 at P_{inj}=300 bar and P_{inj}=360 bar. Distance from the nozzle: 90 mm.

Finally, it can be noticed in Figure 32 that NO concentration seems to drop after reaching the maximum without reaching a constant value. Some measurements later in time would show nitric oxide fluorescence stabilization.

5 Conclusions

In the light of these results, first it can be concluded that attenuation represents a major problem in NO laser induced fluorescence. Either stronger laser signals or better attenuation correction models are necessary to perform more accurate measurements in the A←X (0, 0) excitation bands. As it was reported, other schemes can reduce attenuation, but the fluorescence emitted is weaker.

The oxygen atom of the DME molecule might play an important role in the nitric oxide formation, making it more uniform along the flame plume than in other fuels. However, the main formation areas are placed in the lean regions in the contour of the flame, far from the nozzle, due to the presence of nitrogen and oxygen from air. The spray at that point is fully developed and the mixing and vaporization is faster.

Most of the NO is formed late after start of injection, when the combustion process has almost finished. At this point, the temperature in the flame is very high and chemical reactions have had some more time to occur. From all this, it can be concluded that Zeldovich mechanism seems to be the predominant NO formation mechanism in the DME flame

No conclusions can be drawn about the effect of increasing the injection pressure in 6 MPa because of the high uncertainty in the measurements. More measurements are necessary to reduce this and quantify the effect of a higher pressure in the NO concentration.

6 Future work

First, models have to be developed to correct the attenuation reported as the main problem in the measurements. Reducing the signal to noise ratio of the measurements is important as well to draw more conclusions. One good way to do this is to proceed as it was shown in Figure 21, so that the oxygen interference can be reduced.

A qualitative study like the one described in this report, which tries to explain how the NO is formed in a DME flame, is only a starting point, but it provides good understanding. The next step must be correlating it with other variables and a quantitative analysis of the data to extract the NO density from the fluorescence intensity.

In order to do that, several models have already been developed relating fluorescence and NO population (like the one shown in Equation 6). A good model proposed, to derive it, is governed by the following equation:

$$F = C_{\exp}(\lambda) \cdot \Phi(T, p) \cdot g\left(\vartheta_{las}(T, p), \vartheta_{abs}\right) \cdot I_{las} \cdot A \cdot f(T) \cdot \rho_{NO} \quad (18)$$

However, it involves knowing parameters hard to quantify like the local temperature in the flame (T), the quenchers molar fraction (χ_i) along the flame and their collisional cross sections (σ_i), etc. in order to calculate the Stern-Volmer factor (Φ). This can be measured using advanced optical methods or CFD simulations with chemical combustion models.

On the other side, as it has been reported, NO fluorescence is affected by combustion conditions such as injection pressure (studied in this report), chamber pressure or mean temperature in the chamber. Further experiments should be performed to understand how these parameters affect its formation in DME flames.

The next step would be performing bringing those experiments to an optical engine where the conditions differ so much from the combustion chamber, and comparing DME with other fuel to see if it can replace them while meeting legal requirements regarding local emissions. Understanding how the pollutants are formed is the first step to reduce them.

7 Appendix

7.1 UG5 filter

UG5 is the commercial designation for the optical filter whose spectrum is shown in Figure 35:

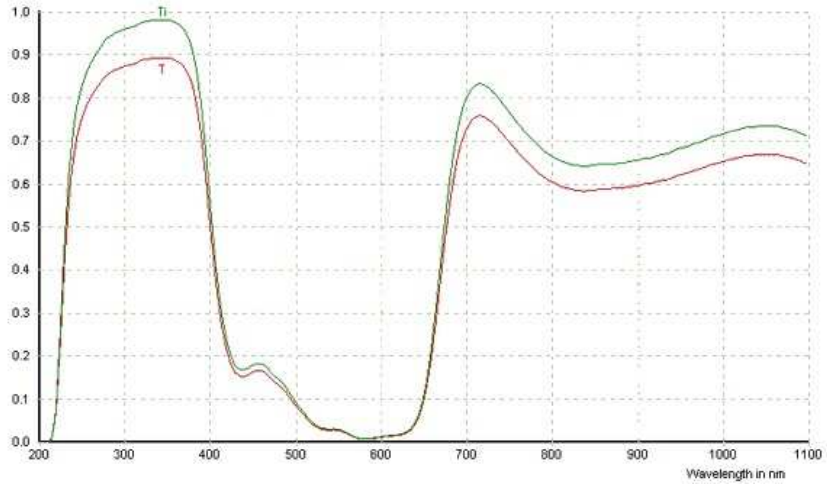

Figure 35. Transmittance of a UG5 filter: The green line corresponds to the internal transmittance, whereas the red line corresponds to the total transmittance.

7.2 Picture of the experiment layout

A picture of the experimental layout is shown in Figure 36:

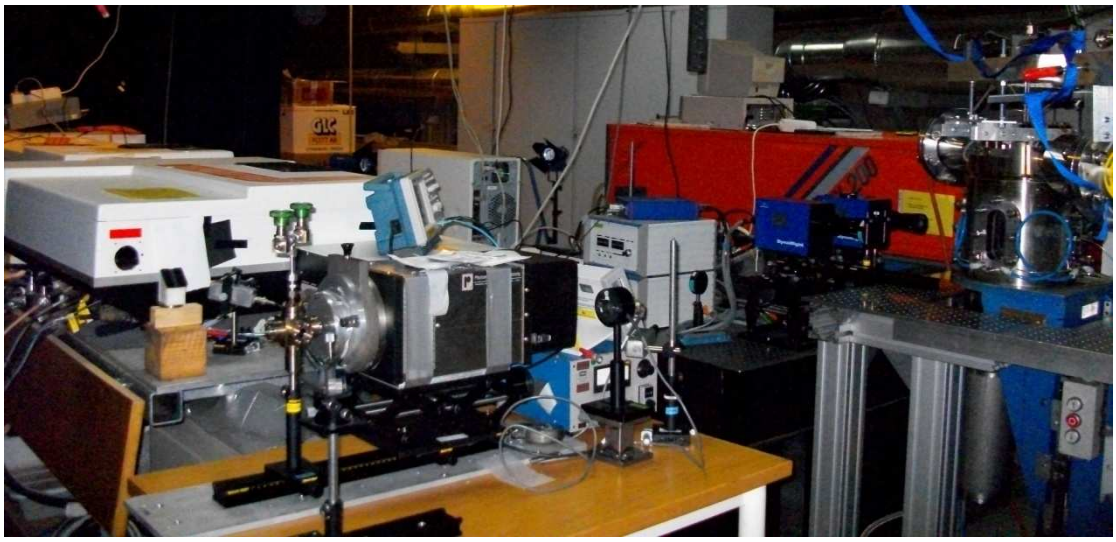

Figure 36. Corner view of the experiment layout.

8 References

[1] Eckbreth, Alan C. (1988): *Laser diagnostics for combustion temperature and species*. Combustion Science & Technology Book Series. Volume 3.

[2] Demory, Romain (2007): *Optical Measurement of Nitric Oxide and Hydroxyl Radicals in Combusting Diesel Sprays*. PhD Thesis. University of Brighton (UK).

[3] Stoffels, Genie Gertruda Maria (1999): *Nitric oxide in a Diesel engine: Laser-based detection and interpretation*. Thesis Katholieke Universiteit Nijmegen.

[4] Rabadán, I.; Tennyson J.: *Ab initio potential energy curves of Rydberg, valence and continuum states of NO.*

[5] Banwell, C. N.; McCash, E. M. (1994): *Fundamentals of Molecular Spectroscopy*, McGraw–Hill.

[6] Rosa, Michael D. Di, Klavuhn, Kurt G. and Hanson, Ronald K. (1996): *LIF Spectroscopy of NO and O2 in High Pressure Flames*. Combustion Science and Technology, 118: 4, 257 – 283

[7] Andresen, P., Bath, A., Gröger, W., Lülf, H., Meijer, G. and Ter Meulen, J. J. (1988): *Laser induced fluorescence with tunable excimer lasers as a possible method for instantaneus temperature field measurements at high pressures*. Applied Optics, 27, 365-378.

[8] Schulz, C.; Yip, B.; Sick, V.; And Wolfrum, J.: *A laser induced fluorescence scheme for imaging nitric oxide in engines*. Physkalisch–Chemisches Institut, Universität Heidelberg, Im Neuenheim Feld 253, D-69120, Heidelberg, Germany.

[9] Bessler, W. G.; Schulz, C.; Lee, T.; Jeffries, J. B. and Hanson, R. K. (2002): *Strategies for laser induced fluorescence of nitric oxide in high pressure flames. I A-X(0,0) excitation.*

[10] Bessler, W. G.; Schulz, C.; Lee, T.; Jeffries, J. B. and Hanson, R. K. (2003): *Strategies for laser induced fluorescence of nitric oxide in high pressure flames. II A-X(0,1) excitation.*

[11] Bessler, W. G.; Schulz, C.; Lee, T.; Jeffries, J. B. and Hanson, R. K.: *Strategies for laser induced fluorescence of nitric oxide in high pressure flames. III Comparison of A-X excitation schemes.*

[12] Dec, J. E. (1997): *A conceptual model of DI Diesel combustion based on laser sheet imaging.* SAE paper 970873.

[13] Heywood, J. B. (1988): *Internal combustion engine fundamentals*.McGraw–Hill.

[14] Kim, Tae-Hyun; Kim, Jong-Min; Hwang, Cheol-Hong; Kum, Sung-Min and Lee, Chang-Eon (2009): *The effect of chemical structure of dimethyl ether (DME) on Nox formation in nonpremixed counterflow flames*.

[15] Cipolat, D. (2007): *Analysis of energy release and NOx emissions of a CI engine fuelled on Diesel and DME*.

[16] Bessler, Wolfgang G.; Schulz, Christof; Sick, Volker and Daily, John W. (2003): *A versatile modeling tool for nitric oxide LIF spectra*.

[17] Battles, Brett E.; Hanson, Ronald K. (1994): *Laser induced fluorescence measurements of NO and OH mole fraction in fuel-lean high-pressure (1-10 atm)*

methane flames: fluorescence modelling and experimental validation. Stanford University, Stanford CA 94305–3032, USA.

[18] Hatsuzawa, H.; Oguma, M.; Goto, S. (2004): *Spectroscopic Analysis of Combustion in the DME Diesel Engine.*

[19] Kuti, O. A.; Xiangang, W. G.; Zhang W.; Nishida, K.; Zhang, Z. H.(2010): *Characteristics of the ignition and combustion of biodiesel fuel spray injected by a common-rail injection system for a direct-injection diesel engine.*

[20] Wu, Junhua; Huang, Zhen; Quiao, Xinqi; Lu, Jun; Zhang, Janjan; Zhang, Liang, (2008): *Study of combustion and emission characteristics of turbocharged diesel engine fuelled with dimethylether.*